

# De-biased Populations of Kuiper Belt Objects from the Deep Ecliptic Survey

E. R. Adams<sup>1</sup>, A. A. S. Gulbis<sup>2,3</sup>, J. L. Elliot<sup>3,4</sup>, S. D. Benecchi<sup>1,5</sup>, M. W. Buie<sup>6</sup>, D. E. Trilling<sup>7</sup>, and L. H. Wasserman<sup>8</sup>

## ABSTRACT

The Deep Ecliptic Survey (DES) was a survey project that discovered hundreds of Kuiper Belt objects from 1998-2005. Extensive follow-up observations of these bodies has yielded 304 objects with well-determined orbits and dynamical classifications into one of several categories: Classical, Scattered, Centaur, or 16 mean-motion resonances with Neptune. The DES search fields are well documented, enabling us to calculate the probability on each frame of detecting an object with its particular orbital parameters and absolute magnitude at a randomized point in its orbit. The detection probabilities range from a maximum of 0.32 for the 3:2 resonant object 2002  $GF_{32}$  to a minimum of  $3 * 10^{-8}$  for the highly-eccentric Scattered object 2003  $FH_{127}$ . By grouping individual objects together by dynamical classes, we can estimate the distributions of four parameters that define each class: semi-major axis, eccentricity, inclination, and object size. The orbital element distributions ( $a$ ,  $e$ , and  $i$ ) were fit to the largest three classes (Classical, 3:2, and Scattered) using a maximum likelihood fit. Using the absolute magnitude ( $H$ -magnitude) as a proxy for the object size, we fit a power

---

<sup>1</sup>Planetary Science Institute, 1700 East Fort Lowell, Suite 106, Tucson, AZ 85719

<sup>2</sup>The Southern African Large Telescope and South African Astronomical Observatory, Cape Town, South Africa, 7935

<sup>3</sup>Department of Earth, Atmospheric, and Planetary Sciences, Massachusetts Institute of Technology, 77 Massachusetts Ave., Cambridge, MA, 02139

<sup>4</sup>Deceased

<sup>5</sup>Carnegie Institution of Washington, Department of Terrestrial Magnetism, 5241 Broad Branch Road NW, Washington, DC 20015-1305

<sup>6</sup>Southwest Research Institute, 6220 Culebra Road, San Antonio, TX 78238, USA.

<sup>7</sup>Department of Physics & Astronomy, Northern Arizona University, S San Francisco St, Flagstaff, AZ 86011, USA

<sup>8</sup>Lowell Observatory, 1400 W. Mars Hill Rd., Flagstaff, AZ 86001

law to the number of objects vs.  $H$  magnitude for 8 classes with with at least 5 detected members (246 objects). The Classical objects, which have observed values from  $5 \leq H \leq 7.2$ , are best fit with a power-law slope of  $\alpha = 0.989 \pm 0.011$ . The *slopes* of the magnitude distributions for the seven next most populated dynamical classes (Scattered, Centaur, and 5 resonances) are consistent with the power-law relation of the Classicals, provided that the *absolute number* of objects is scaled. Scattered objects are approximately as numerous as Classical objects, while there are only a quarter as many 3:2 objects as Classicals. The exception to the power law relation is the Centuars, non-resonant objects with perihelia closer than Neptune, which are therefore brighter and detectable at smaller sizes. Centaurs were observed from  $7.5 < H < 11$ , and the population is best fit by a power law with  $\alpha = 0.44 \pm 0.04$ . Based on the Classical-derived magnitude distribution, the total number of objects ( $H \leq 7$ ) in each class are: Classical ( $2200 \pm 400$  objects), Scattered ( $2200 \pm 400$ ), 3:2 ( $550 \pm 100$ ), 2:1 ( $330 \pm 60$ ), 5:2 ( $550 \pm 100$ ), 7:4 ( $66 \pm 12$ ), 5:3 ( $66 \pm 12$ ). The independent estimate for the number of Centaurs in the same  $H$  range is  $15 \pm 14$ .

*Subject headings:* Kuiper Belt – methods: data analysis– solar system: formation – solar system: general – surveys

## 1. Introduction

Studies of the Kuiper Belt have progressed in the last two decades from finding individual objects (Jewitt and Luu 1993) to estimating the total number of objects in the outer solar system through observations and statistics (e.g. this work; Petit et al. 2011; Gladman et al. 2012). The Kuiper Belt itself has been subdivided into many distinct dynamical classes of objects, including objects in mean-motion resonances with Neptune, high and low inclination populations (Hot vs. Cold Classical, e.g. Morbidelli et al. 2008) and various groupings of scattered objects that have undergone dynamical interactions with Neptune. The relative numbers of objects in all of these populations offer one of the best direct observational constraints on different dynamical models of solar system formation and evolution.

A recent renaissance in modeling has resulted in a number of mostly successful attempts to reproduce the architecture of the solar system. Scattering and migration of giant planets should leave directly observable signatures in the dynamical structure and numbers of small bodies remaining in the asteroid and Kuiper Belts and the outer satellites (Levison et al. 2008; Morbidelli et al. 2009; Bottke et al. 2012). Some models, such as the Nice Model (Gomes et al. 2005; Morbidelli et al. 2005; Tsiganis et al. 2005) and the “Grand

Tack” (Walsh et al. 2012), invoke large-scale, abrupt motion by the giant planets. Other models, based on smooth migration of the giant planets, predict different ratios of objects captured into mean-motion resonance with Neptune (Malhotra 1993; Hahn and Malhotra 2005).

Most models to date can successfully account for some – but not all – features of the Kuiper Belt, such as reproducing the Cold but not the Hot Classical populations, or leaving particular resonances over- or under-populated relative to the apparent populations. Observational constraints can be used to distinguish between models and resolve fundamental questions, such as how Neptune migrated outward: smoothly on a nearly circular orbit (e.g. Hahn and Malhotra 2005), through dynamic scattering with potential high eccentricity which was later damped down (e.g. Levison et al. 2008; Walsh et al. 2012), or some other model. This fundamental debate is evident in recent meetings, where one presentation concluded that chaotic migration models are more likely based on colors of resonant Kuiper Belt Objects, or KBOs (Sheppard 2012), while another claimed that smooth migration models are preferred based on observations of the binary fraction (Noll et al. 2012).

Until recently, however, comparisons to observations have been disadvantaged because the known sample (over 1600 objects) is an inherently biased population, due to the difficulty of obtaining observations of faint, distant objects. What is needed is a de-biased population of objects, that is to say, a relatively large sample of objects discovered by a wide-field, all-sky survey that have had the sources of bias accounted for and removed. Two surveys with the best and largest samples have recently begun to provide such results. The Canada-France Ecliptic Plane Survey (CFEPS), with a sample of 169 objects with high-quality orbits, reported de-biased population estimates in Petit et al. (2011) and Gladman et al. (2012).

Here we report the results of the Deep Ecliptic Survey (DES) (Millis et al. 2002; Elliot et al. 2005), the largest single survey to date, which has discovered about 500 objects with provisional designations by the Minor Planet Center (MPC). Of these objects, 304 have high-quality orbits suitable for dynamical classifications. The de-biased class populations presented in this paper offer a completely independent check on the CFEPS results, on both the absolute and relative numbers of objects, since the DES uses a different set of objects and discovery fields and a new approach to de-biasing. The DES sample also more than doubles the number of de-biased objects available, particularly in the small-number classes of high-order resonances and Scattered objects. Finally, we hope that the approach described in this paper will be useful for obtaining uniformly de-biased results of the expected thousands or tens of thousands of objects found by future large-scale surveys, such as Pan-STARRS (Grav et al. 2011) and the Large Synoptic Survey Telescope (LSST, Ivezić et al. 2008).

In Section 2 we describe the data and briefly review the choice of classification scheme.

In Section 3 we present the analytical framework for calculating the detection probabilities. Section 4 contains the numerical implementation of the detection probabilities and the methods used to estimate the number of objects in each class. In Section 5 we compare our results to other surveys. In Section 6 we relate our observations to theories of planetary formation.

## 2. Observations

A full description of the DES can be found in Millis et al. (2002) and Elliot et al. (2005) (henceforth E05), but the relevant details are summarized here. The DES was an NOAO (National Optical Astronomical Observatory) survey. Two 4-meter telescopes (the Mayall at Kitt Peak in Arizona and the Blanco at Cerro Tololo in Chile) were used, with identical Mosaic cameras with 8 SITe CCD chips, each chip measuring 4096 by 2048 pixels. Each mosaic image covers about  $0.35 \text{ deg}^2$  on the sky. Each field was within  $\pm 6.5^\circ$  of the ecliptic and was selected to have at least 35 USNO-B astrometric reference stars on each chip. The fields were also chosen to exclude stars brighter than magnitude  $V = 9.5$  (Millis et al. 2002). Typically two 300-sec exposures would be taken on the same night a few hours apart, with a third frame on another night during the same observing run. This resulted in orbital arcs of at least 24 hours (required for a designation by the MPC). Most of the fields imaged were distinct, but sometimes frames of the same field taken several years apart were counted as new search fields, since by that time a new set of objects would have moved into the field area. In 2005, the Deep Ecliptic Survey stopped surveying new fields, although recovery efforts to improve orbits and classifications of known objects have continued.

In order to obtain as uniform a sample as possible, for this work several selection criteria were applied to both the search fields and the objects discovered by the DES, as described below.

### 2.1. Search frame selection

The discovery phase of the DES ended on 11 May 2005. A few KBOs were discovered during subsequent recovery efforts, but are not included in our sample since they were found under different search conditions. (For objects that were discovered during the main survey, we used the latest available orbital information to assign dynamical classes and calculate discovery probabilities.)

A total of 62,392 individual frames are in the DES database, corresponding to one of the eight CCD detectors on the Mosaic camera. Of these, 14,440 were not suitable for de-biasing

because these frames were specifically targeted at the recovery of particular objects. Targeted recovery frames were not held to the same criteria for the number and brightness of stars, and have different statistical properties. An additional 1,312 frames with solar elongation angle less than  $140^\circ$  were eliminated, because they have a different search efficiency than the bulk of the frames, which were taken nearer to opposition. (Over twice as many objects were found on high solar elongation frames than on low-elongation frames.) This left 46,640 individual frames.

Each field was observed at least three times: a pair of images taken on the same night a few hours apart, and one more image on another night. Sometimes additional frames were taken, for instance if weather interrupted the original observations. Only the pair of frames on the same night was used to search for objects. There were 18,668 pairs of frames that met these criteria. The overlap fraction for each pair is quite high, with a median positional offset of  $0.026''$ . Each frame is  $1065''$  by  $532''$ , and the largest mis-registration was less than  $80''$  in RA and less than  $90''$  in declination.

## 2.2. Object selection

As of 2012 August, a total of 913 KBOs were listed in the DES internal database. Some objects have been excluded from this analysis because they were found outside of the main survey, during recovery or other follow-up observations (101 objects). We also exclude 8 objects found on low solar elongation fields ( $< 140^\circ$ ). Several additional objects, typically those that were lost shortly after discovery, are excluded because of missing information: objects lack discovery field coordinates (36 objects), discovery distances (104 objects), or discovery magnitudes (1 object). This leaves 663 objects discovered during the main DES survey.

Of these objects, 478 objects had sufficient observations post-discovery to receive preliminary designations from the Minor Planet Center (72%). Dynamical classification typically requires additional observations to achieve low enough errors, and 316 objects (48%) have been classified (see Section 2.3). Almost all (304) of these classifications are considered to be secure (quality 3 as defined in E05). For our analyses, we used the 304 securely classified DES objects.

### 2.3. Dynamical Classification

Over the years, several different schema for dynamically classifying KBOs have been proposed (e.g. Elliot et al. 2005; Lykawka and Mukai 2007; Gladman et al. 2008). In this paper, we use the current DES classification scheme, a modified version of the scheme laid out in E05 which incorporates the Scattering concept from Gladman et al. (2008). Since differences in the precise definitions of classes can affect the membership of objects at the edges, we describe our classification scheme in full below.

To test for the dynamical class of an object, we use both the current observed orbital parameters as well as a 10 Myr integration of the orbit forward in time, and two additional 10 Myr integrations for the  $\pm 3 \sigma$  values for  $a$ ,  $e$ , and  $i$ . An object is said to be securely classified (quality 3) only if all three integrations agree on the same dynamical class. (In quality 2 objects, the nominal classification only agrees with one of the  $+3 \sigma$  or  $-3 \sigma$  integrations, while in quality 1 it agrees with neither.)

An object is tested for membership in each of the following dynamical classes, in order. (1) *Resonant* objects occupy a mean-motion resonance with Neptune (resonances up to ninth order are tested). (2) *Centaur*s have osculating perihelia that reach values less than the osculating semimajor axis of Neptune. (3) *Scattered Near* objects, have  $a$  values that vary by more than an arbitrary amount,  $\Delta a \geq 0.02$ , over the 10 Myr integration (where  $\Delta a = (a_{max} - a_{min})/a_{mean}$ ). This is along the same lines as the Scattering class of Gladman et al. (2008), which uses  $a_{max} - a_{min} > 1.5$  AU. An excitation statistic,  $s = \sqrt{e^2 + \sin(i)^2}$ , is applied to the remaining objects, which are sent to two additional classes: (4) *Scattered Extended* objects have  $s \geq 0.25$ , and (5) *Classical* objects have  $s < 0.25$ .

For the purposes of this paper, we have re-grouped a few objects in order to be more broadly consistent with the classes used by CFEPS and elsewhere. First, we restrict the population of Centaurs to only those with semi-major axes less than Neptune’s (resulting in a population of smaller objects than found in any other class, due to the magnitude bias toward finding closer objects). Second, we group all of the dynamically excited objects with  $a_{Nep} \leq a \leq 80$  AU into a single *Scattered* class, which contains objects from the Centaur, Scattered-Near, and Scattered-Extended classes. Ten objects with  $a = 82 - 739$  AU are not considered in this analysis, because they are too sparse in parameter space to adequately define a dynamical class; for a brief discussion of such rare objects see Section 5.3.

### 3. Analytical framework

We now consider how we can use the sample of KBOs discovered by the DES to learn about the entire population of KBOs. Dynamical classes for KBOs have been defined with the underlying assumption that the members of each class have experienced a common formation process and common dynamical evolution. Hence, we shall consider the objects in each dynamical class separately. Within a dynamical class, we assume that the DES discoveries give us a sampling of the greater population of the objects, which can be characterized by four distribution functions: one each for the  $H$ -magnitude, semimajor axis  $a$ , eccentricity  $e$ , and inclination  $i$ .

In Section 3.1, we develop the equations to compute the probability of detection by the DES for each object, as a function of  $H$ ,  $a$ ,  $e$ , and  $i$ . In Section 3.2, we present the distribution functions that we assume are followed by the general population of the dynamical class for the same four parameters. Finally, in Section 3.3 we develop a maximum likelihood model to fit the data. From this fit, we determine, with error bars, the parameters of the four distribution functions and the number of objects in each dynamical class, within the range of orbital parameters probed by the DES discoveries. We have chosen to apply the maximum-likelihood technique directly, rather than applying least-squares fitting to binned data, since the objects per bin are sparse in the four-dimensional  $H$ ,  $a$ ,  $e$ , and  $i$ -space (see Chapter 10 of Bevington and Robinson 2003).

#### 3.1. Probabilities of Detection

To compute the probability that an object would have been detected by the DES at some time during the survey, we extend the methods described in E05 to include observational biases introduced by an object's  $H$ ,  $a$ ,  $e$ , and  $i$ . We refer all inclinations to the Kuiper Belt plane (KBP), as derived in E05 ( $i = 1.74^\circ \pm 0.23$ ,  $\Omega = 99.2^\circ \pm 6.6$ ), which is consistent with the invariable plane of the solar system at the  $1\text{-}\sigma$  level. Following the approach used in E05, we consider a set of  $N_O$  objects ( $j = 1, \dots, N_O$ ) discovered in a set of  $N_F$  search fields ( $k = 1, \dots, N_F$ ). For the  $j$ th object discovered by the survey, we denote its  $H$ -magnitude, semimajor axis, eccentricity, and inclination by the symbols  $H_j$ ,  $a_j$ ,  $e_j$  and  $i_j$ . We assume that the  $H$  magnitude of an object is not correlated with its orbital elements, and that angles that describe the orientation of the orbit in 3-dimensional space average out over time.

Each of the  $N_F$  fields of the survey data set is characterized by (i) the magnitude for which the detection efficiency has dropped to  $1/2$ , which we denote by  $m_{1/2,k}$ , (ii) the Kuiper Belt latitude and tilt of the frame ( $\beta_K$  and  $\theta_K$ ), (iii) the Kuiper Belt longitude of the frame

( $\lambda_K$ ), and (iiv) the solid angle,  $\Omega_k$ , subtended by the search field. Below we describe how biases related to all four of these characteristics have been removed.

(i) We assume that all search fields have the same maximum efficiency at bright magnitudes,  $\epsilon_{max}$ , and the same characteristic range,  $\sigma_m$ , over which the detection efficiency drops from  $\epsilon_{max}$  to 0. For the  $k$ th search field, we employ the functional form used by Trujillo et al. (2001) and in E05 (their equation 19) for the detection efficiency as a function of magnitude,  $\epsilon(m, m_{1/2,k})$ :

$$\epsilon(m, m_{1/2,k}) = \frac{\epsilon_{max}}{2} \left[ 1 + \tanh \left( \frac{m_{1/2,k} - m}{\sigma_m} \right) \right]. \quad (1)$$

The  $j$ th object has a minimum magnitude,  $m_{min,j}$  and a maximum magnitude,  $m_{max,j}$ . Between these extremes, the relative time that the object is at magnitude  $m$  is given by the probability distribution function  $p_j(m)$  for the  $j$ th object. Hence the likelihood,  $\xi_{mag,j,k}$ , for the  $j$ th object being discovered in the  $k$ th search field due solely to its magnitude (we shall consider other factors later) is given by

$$\xi_{mag,j,k} = \int_{m_{min,j}}^{m_{max,j}} p_j(m) \epsilon(m, m_{1/2,k}) dm. \quad (2)$$

Our strategy for evaluating the integral in Equation 2 involves transforming it from an integral over magnitude to an integral over heliocentric distance. To do this we make several simplifying assumptions. First we assume that all objects are discovered at opposition, and we set the Earth-Sun distance to 1 AU when computing the variation in the opposition magnitude of an object throughout its orbit. We define  $R_{d,j}$  as the heliocentric discovery distance for the  $j$ th object and  $m_{d,j}$  as its discovery magnitude. We neglect photometric variability due to changing phase angle and/or rotational light curve, since the mean amplitude of variability is only 0.1 mag, with only 15% of all KBOs varying by more than 0.15 mag (Thirouin et al. 2010). Then the magnitude of the  $j$ th object at a heliocentric distance  $R$  is given by the equation,

$$m_j(R) = m_{d,j} + 5 \log_{10}(R/R_{d,j}) + 5 \log_{10} [(R - 1 \text{ AU}) / (R_{d,j} - 1 \text{ AU})]. \quad (3)$$

For the  $j$ th object, the minimum and maximum heliocentric distances are  $R_{min,j}$  and  $R_{max,j}$  respectively:

$$R_{min,j} = a_j(1 - e_j), \quad (4)$$



$$R_{max,j} = a_j(1 + e_j). \quad (5)$$

For two-body orbital motion, the time that the  $j$ th object spends at a given heliocentric distance,  $R$ , is proportional to the square of that distance, so the probability distribution of heliocentric distances for the  $j$ th object,  $p_j(R)$ , is

$$p_j(R) = \begin{cases} \frac{3R^2}{2e_j a_j^3 (3+e_j^2)} & \text{if } R_{min,j} \leq R \leq R_{max,j} \\ 0 & \text{otherwise.} \end{cases} \quad (6)$$

We are now in a position to rewrite Equation 2 in terms of an integral over heliocentric distance. Since our approximations reduce the apparent magnitude of an object with a given  $H$  magnitude to only the variation that depends on its semi-major axis and eccentricity, we emphasize this by using the symbol  $\xi_{j,k}(H, a, e)$  for the likelihood factor instead of  $\zeta_{MAG,j,k}$  used in E05 (see the Glossary in their Appendix C). Substituting  $p_j(R)dR$  for  $p_j(m)dm$  in the integral and changing the limits of integration from magnitudes to the corresponding heliocentric distances, we find

$$\xi_{j,k}(H, a, e) = \int_{R_{min,j}}^{R_{max,j}} p_j(R) \epsilon(m_j(R), m_{1/2,k}) dR. \quad (7)$$

Equation 7 can be evaluated with substitutions from Equations 1, 3, and 6, using Equations 4 and 5 to set the limits of integration.

(ii) We now consider the bias factor for inclination,  $\xi_{j,k}(i)$ . The approach used is the same as in the analysis of the inclination distribution in Gulbis et al. (2010), hereafter G10. First we write an expression for the conditional probability of finding an object at latitude  $\beta$  with an inclination  $i$ , which is Equation (9) of G10:

$$p(\beta|i) = \begin{cases} \frac{\cos \beta}{\pi \sqrt{\sin^2 i - \sin^2 \beta}} & \sin i > |\sin \beta| \\ 0 & \sin i \leq |\sin \beta| \text{ \& } i \neq \beta \neq 0 \\ 1 & i = \beta = 0 \end{cases} \quad (8)$$

It is important to note that in G10 and in this work all inclinations and latitudes are taken relative to the Kuiper Belt Plane (KBP).

We define  $\xi_{j,k}(i)$  as the likelihood (based on the inclination alone) of detecting the  $j$ th object in the  $k$ th search field, which we determine by integrating the conditional probability for the inclination,  $i_j$ , over the range of KBP coordinates covered by the  $k$ th search field:

$$\xi_{j,k}(i) = \int_{\beta_{min,k}}^{\beta_{max,k}} \Delta\lambda(\beta'_k, \theta_k) p(\beta'_k | i_j) d\beta'_k, \quad (9)$$

where  $\Delta\lambda$  is the the range of longitudes at each latitude on the frame (a geometric parameter derived in G10, their Equations 11-14), and  $\theta_K$  is the tilt of the frame with respect to the Kuiper Belt plane.

(iii) The bias toward only discovering resonant objects at certain longitudes is accounted for by uniformly weighting all fields with longitudes within the allowed longitude range,  $\lambda_{j,min} \leq \lambda \leq \lambda_{j,max}$ , as determined by the libration amplitude in a 10 Myr integration of the orbit of each object:

$$\xi_{long,j} = \begin{cases} 360/(\lambda_{j,max} - \lambda_{j,min}) & \lambda_{j,min} \leq \lambda \leq \lambda_{j,max} \\ 0 & \text{otherwise} \end{cases}. \quad (10)$$

(iv) A minor correction is included for the solid angle of each set of fields that is available for object searches. The effective search area for a pair of frames varies slightly due to mis-registration (typically a few arcseconds) and obscuration by other objects on the field. Defining  $\Omega_s$  as the solid angle of a full CCD and  $\Omega_k$  as the net solid angle for the  $k$ th CCD, the solid angle component of the likelihood factor (following E05) is

$$\xi_{ang,k} = \Omega_k / \Omega_s. \quad (11)$$

Neglecting any correlation among  $a$ ,  $e$ ,  $i$ , and  $H$ , the combined likelihood,  $\zeta_{j,k}(H, a, e, i)$ , for detecting the  $j$ th object in the  $k$ th search field is the product of the four separate likelihood components in Equations 7, 9, 10, and 11:

$$\zeta_{j,k}(H, a, e, i) = \xi_{j,k}(H, a, e) \xi_{j,k}(i) \xi_{long,j} \xi_{ang,k}. \quad (12)$$

If we would observe all the search fields simultaneously, then the probability for having detected the  $j$ th object for the  $N_F$  search fields would be equal to the sum of the probabilities for each search field. This would be the case for a single night, or even a single lunation. However, we observe the search fields over a period of years, with the possibility of an object moving between search fields, so the efficiency of detecting the objects is 1 minus the product of the likelihoods of having not detected it in each search field. We refer to this quantity as the detection probability of the survey for the  $j$ th object,  $q_{det}(H_j, a_j, e_j, i_j)$ :

$$q_{det}(H_j, a_j, e_j, i_j) = 1 - \prod_{k=1}^{N_F} (1 - \zeta_{j,k}(H, a, e, i)). \quad (13)$$

From the probability of detecting each individual object and other assumptions, we can characterize the distribution of unbiased orbital parameters and estimate the numbers of objects in each of the dynamical classes, as described in the next section.

### 3.2. Distribution Functions for $H$ -Magnitude and Orbital Parameters

The simplest differential  $H$  magnitude distribution function,  $p_H(\alpha, H)$ , is a power law with exponent  $\alpha$ . If  $c_H$  is a normalization constant so that the integral of the distribution function between  $H_{min}$  to  $H_{max}$  is equal to one, then:

$$p_H(\alpha, H) = \begin{cases} c_H 10^{\alpha H} & H_{min} \leq H \leq H_{max}, \\ 0 & H < H_{min} \text{ or } H_{max} < H, \end{cases} \quad (14)$$

where

$$c_H = \frac{\alpha \ln 10}{10^{\alpha H_{max}} - 10^{\alpha H_{min}}}. \quad (15)$$

Next we consider the differential distribution function for semimajor axes. Between the minimum and maximum values of the DES detections we model this distribution function,  $p_a(a_o, \Delta a, a)$ , as a Lorentzian with its central peak offset from zero by  $a_o$  and full-width at half-maximum (FWHM) of  $2\Delta a$ :

$$p_a(a_o, \Delta a, a) = \begin{cases} \frac{c_a}{1 + [(a - a_o)/\Delta a]^2} & a_{min} \leq a \leq a_{max}, \\ 0 & a < a_{min} \text{ or } a_{max} < a, \end{cases} \quad (16)$$

where the normalizing constant,  $c_a$ , is given by

$$c_a = \frac{1}{\Delta a [\arctan((a_{max} - a_o)/\Delta a) - \arctan((a_{min} - a_o)/\Delta a)]}. \quad (17)$$

The distribution of eccentricities is similarly modeled as a single Lorentzian with parameters  $e_o$ ,  $\Delta e$ , and  $c_e$ , using analogous versions of Equations 16 and 17.

We note that the inclination distribution may be represented as a single Lorentzian, using  $i_o$ ,  $\Delta_i$ , and  $c_i$ . However, for the Classical distribution, other more complicated models have been used. Thus we also examined a double-Gaussian model, to represent what may be two populations of objects, the “core” and “halo” populations (Brown 2001; Elliot et al. 2005; Gulbis et al. 2006). To be specific, the first Gaussian component is the narrower one (core) and has a characteristic width (the standard deviation in the Gaussian expression) of  $\Delta_{i1}$ . The second Gaussian component is broader (halo) with a characteristic width  $\Delta_{i2} > \Delta_{i1}$ . We normalize each component separately, and  $b$  is a number between zero and one, representing the fraction of objects in the narrower Gaussian component. The inclination distribution function,  $p_i(b, \Delta_{i1}, \Delta_{i2}, i)$ , can be written as:

$$p_i(b, \Delta_{i1}, \Delta_{i2}, i) = \begin{cases} \frac{bc_{i1}}{\sqrt{2\pi\Delta_{i1}^2}} \exp \frac{-i^2}{2\Delta_{i1}^2} + \frac{(1-b)c_{i2}}{\sqrt{2\pi\Delta_{i2}^2}} \exp \frac{-i^2}{2\Delta_{i2}^2} & i_{min} \leq i \leq i_{max} \\ 0 & i < i_{min} \text{ OR } i_{max} < i \end{cases}. \quad (18)$$

The normalizing constants,  $c_{i1}$  and  $c_{i2}$ , are given by:

$$c_{i1} = \frac{1}{I(\Delta_{i1}, i_{max}) - I(\Delta_{i1}, i_{min})} \text{ and } c_{i2} = \frac{1}{I(\Delta_{i2}, i_{max}) - I(\Delta_{i2}, i_{min})}, \quad (19)$$

where the integral,  $I(\Delta, i)$  is given by the error function (erf):

$$I(\Delta, i) = \frac{1}{2} \operatorname{erf} \left( \frac{i}{\sqrt{2}\Delta} \right). \quad (20)$$

The distributions are normalized over the expected range of parameters. The  $e$  and  $i$  values are normalized over the full range of parameter space ( $e = 0 - 0.95$  to avoid hyperbolic orbits, and  $i = 0 - 170^\circ$  to avoid numerical effects around 180 degrees; the effect of stopping the integrals slightly short of the full range was insignificant). For the  $a$  values, we used the minimum and maximum observed values in each class: the distribution of 3:2 objects is shaped by dynamics, and we do not expect it to continue outside of the observed range of semi-major axes ( $a = 39 - 40$  AU), while for the Classical and Scattered classes enough objects are observed far from the main peak of objects that a difference in a few AU on either side has little effect on the normalization. The  $H$  distributions, which are power laws, are normalized only over the range of objects modeled.

### 3.3. Maximum Likelihood

We can now use the defined distribution functions with classes of real objects. First, we model the data with maximum likelihood (ML) to determine the parameters for the distribution functions for  $H$ ,  $a$ ,  $e$ , and  $i$ . We can then use the ML solution to estimate the actual number of objects.

#### 3.3.1. Distribution Function Parameters

For a given dynamical class, the likelihood function for the distribution function parameters,  $L$ , is given by a product for all objects of the probability density functions, raised to the inverse power of the detection probability for that object:

$$L = \prod_{j=1}^{N_0} [p_H(\alpha, H_j) p_a(a_o, \Delta_a, a_j) p_e(e_o, \Delta_e, e_j) p_i(b, \Delta_{i1}, \Delta_{i2}, i_j)]^{1/q_{det}(H_j, a_j, e_j, i_j)}. \quad (21)$$

Computationally, it is easier to maximize the natural logarithm of  $L$ , which we define as  $M$  :

$$M = \sum_{j=1}^{N_0} \frac{\ln [p_H(\alpha, H_j) p_a(a_o, \Delta_a, a_j) p_e(e_o, \Delta_e, e_j) p_i(b, \Delta_{i1}, \Delta_{i2}, i_j)]}{q_{det}(H_j, a_j, e_j, i_j)} \quad (22)$$

To calculate the errors, we assume that the number of objects in the sample is great enough so that the formal errors on the ML estimates approximately follow a Gaussian distribution, using the method of Crooke et al. (1999). We define the matrix  $\mathbf{X}$  as a  $j \times n$  matrix, where there are  $j$  objects and  $n$  parameters (e.g.,  $\alpha, a_o, \Delta_a, e_o, \Delta_e, b, \Delta_{i1}, \Delta_{i2}$  with a double-Gaussian inclination model). Each element  $X_{j,n}$  is given by the expression:

$$X_{j,n} = \left. \frac{\delta M}{\delta x_m} \right|_{H=H_j, a=a_j, e=e_j, i=i_j}. \quad (23)$$

The correlation matrix,  $\mathbf{C}$ , can be expressed in terms of  $\mathbf{X}$ :

$$\mathbf{C} = [\mathbf{X}^T \mathbf{X}^{-1}]. \quad (24)$$

The variance of the parameter  $x_n$  is given by the appropriate diagonal element,  $C_{n,n}$ , of the correlation matrix, and the standard deviation is found by taking the square root:

$$\sigma_n = \sqrt{C_{n,n}}. \quad (25)$$

### 3.3.2. Inferred Number of Objects

Once we have determined the unknown parameters for all of the distribution functions, we can then estimate the number of objects in the class, again using ML. Within the minimum and maximum values of  $H$ ,  $a$ ,  $e$ , and  $i$  that we have specified for our ML solution for the distribution-function parameters, we assume that the total population for a given dynamical class is well described by the distribution functions. Given that assumption, we can calculate the fraction of the total population,  $f$ , where  $0 \leq f \leq 1$ , that should have been detected by the DES by integrating the distribution functions over the detection probability of an object with the given parameters:

$$f = \int_{H_{min}, a_{min}, e_{min}, i_{min}}^{H_{max}, a_{max}, e_{max}, i_{max}} q_{det}(H, a, e, i) p_H(\alpha, H) p_a(a_o, \Delta_a, a) p_e(e_o, \Delta_e, e) p_i(b, \Delta_{i1}, \Delta_{i2}) dH da de di. \quad (26)$$

To turn the discovered fraction of objects into an estimated total number of actual objects, with error bars, we use the generalized binomial distribution, along with another ML function, where the observed number is  $N_o$  and the actual number of objects is  $N'_o$ :

$$L(N'_o) = \frac{N'_o!}{N_o!(N'_o - N_o)!} f^{N_o} (1 - f)^{N'_o - N_o} = \frac{\Gamma(N'_o + 1)}{\Gamma(N_o + 1)\Gamma(N'_o - N_o + 1)} f^{N_o} (1 - f)^{N'_o - N_o} \quad (27)$$

and thus

$$M(N'_o) = \ln \left[ \frac{\Gamma(N'_o + 1)}{\Gamma(N_o + 1)\Gamma(N'_o - N_o + 1)} \right] + N_o \ln f + N'_o - N_o \ln(1 - f). \quad (28)$$

The number of objects,  $N'_o$ , is found by maximizing Equation 28, while the error is found by numerically calculating the total derivative:

$$\sigma(N'_o) = 1 / \sqrt{\left| \frac{dM(N'_o)}{dN'_o} \right|}. \quad (29)$$

## 4. Numerical implementation

### 4.1. Calculating detection probabilities

Numerical implementation was done using Mathematica 8.0 and python. Equation 13 gives the probability of detecting an object with an orbit described by  $a$ ,  $e$ , and  $i$ , an absolute  $H$ -magnitude, and which was discovered with magnitude  $m_d$  at distance  $R_d$ . Values for  $a$ ,  $e$ ,  $i$ , and  $H$  listed in the DES database in March 2012 were used in these calculations.

Although 304 DES objects have the highest quality orbital classification, we restrict our sample to the 273 objects discovered with a  $VR$  magnitude of 23 or brighter. The nominal 50% detection efficiency of the DES determined by E05 was  $VR = 22.5$ , with  $VR = 23$  corresponding to an efficiency of 15%. The original photometric calibration of the DES (used in this and previous work) was based on the USNO-B1.0 catalog, which is however known to have magnitude uncertainties up to 0.5 mag. Recent recalibration of the DES (Buie et al. 2011) has been completed but not yet reapplied to the survey results. Future work using the revised photometry will have much more reliable magnitudes, particularly for objects detected at the faint edge of the DES’s range. Until the re-calibrated data is available, we have restricted the de-biasing analysis to objects with  $VR \leq 23$ . Table 1 shows the number of objects the DES found in each dynamical class, as well as the breakdown for objects with  $m_d \leq 23$  and additional  $H$ -magnitude constraints used in subsequent fits to single power laws. Three non-resonant classes (Centaur, Classical, and Scattered) and sixteen resonances (five with  $\geq 5$  objects) have been identified for the following analysis.

The detection probabilities (Equation 13) have been calculated for all objects with secure orbits, as shown in Column 2 in Table 2. The probabilities range from a maximum of 0.32 for the 3:2 resonant object 2002  $GF_{32}$  to a minimum of  $3 * 10^{-8}$  for the distant ( $a = 739$ ), highly-eccentric ( $e = 0.95$ ) Scattered object 2003  $FH_{127}$ . (Similar low probability objects are discussed in Section 5.3.)

### 4.2. Estimating size distribution

Determining the size distribution of Kuiper Belt objects first requires a substitution: the  $H$  magnitude of an object, which is easily derived from the observations, is used instead of the actual object diameter, which is usually unknown and can only be estimated with assumptions about an object’s physical properties, such as the albedo (which varies widely among Kuiper Belt objects, Stansberry et al. 2008). One goal is to determine the  $H$ -magnitude distribution for individual dynamical classes, to determine if the size distributions

are the same across objects with different collisional histories.

#### 4.2.1. Power law fits from probability-weighted CDF

A simple method to estimate the number of objects in a class is to convert the probability of detection into a predicted number of actual objects. A probability-weighted cumulative distribution of the estimated number for real objects,  $N$ , brighter than a particular  $H$  magnitude, where there are  $N_o$  observed objects, is calculated by summing the inverse of the detection probability,  $P_N$ :

$$N(\leq H) = \sum_{j=1}^{N_o} \frac{1}{q_{det,j}}. \quad (30)$$

For a given class  $x$  and some normalization scale  $C_x$ , the CDF can be fit with a power law of the form

$$N_x(\leq H) = C_x 10^{\alpha_x H}. \quad (31)$$

A single power law slope has been shown to break down when the range of  $H$ -magnitudes is large enough (Jewitt et al. 1998; Gladman et al. 2001; Bernstein et al. 2004; Fuentes and Holman 2008; Fraser and Kavelaars 2008; Shankman et al. 2013). This is evident in a turnover to a shallower slope, and can be mathematically described by introducing two slopes,  $\alpha_1$  brighter than a certain  $H$ -magnitude, referred to as the break,  $H_b$ , and  $\alpha_2$  for fainter objects:

$$N_x(\leq H) = \begin{cases} C_x 10^{\alpha_1 H} & H \leq H_b \\ C_x 10^{\alpha_1 H_b} 10^{\alpha_2 (H - H_b)} & H_b < H \end{cases}. \quad (32)$$

A plot of the probability-weighted CDF for each class is shown in Figure 1. We examined eight classes with sufficient numbers of objects: Classical, Scattered, Centaur, 2:1, 3:2, 5:2, 5:3, and 7:4. We required that each class have  $N_o \geq 5$  objects with  $m_d \leq 23$ , to avoid problems with sparse sampling at faint magnitudes (note that similar results are obtained using  $m_d \leq 23.5$ ). Similarly, a few objects in the Scattered class were discovered at such great distances (hundreds of AU) that they distort any population fit due to sparse sampling and orders-of-magnitude lower probabilities of discovery; all objects with  $a > 80$  AU are excluded from class analyses.



A single power law cannot explain the full distribution of objects. The location of the turnover to a shallower slope was estimated by examining the two most populous classes, Classical and 3:2. The single power-law fit with the lowest relative error has a break in slope at  $H \leq 7.2$  in both classes, though it is clearer in the Classical objects, since the 3:2 objects have more scatter both at high and low  $H$  objects. The slope for objects with  $H < 7.2$  is  $\alpha = 0.989 \pm 0.011$  from the Classical data and  $0.986 \pm 0.041$  from the 3:2 data ( $5 \leq H \leq 7.2$  after removing the two brightest 3:2 objects; no Classical objects have  $H < 5$ ). A fit to several break points from 6.5 to 7.5 is shown in Figure 2.

We note that break points are commonly seen at the faint edge of observational data, although the absolute value of the break may vary. Fuentes and Holman (2008) observed objects spanning the break, which they placed at  $R = 24.3$  with a slope of  $\alpha_1 = 0.7_{-0.1}^{+0.2}$  before and  $\alpha_2 = 0.3_{-0.3}^{+0.2}$  after. This corresponds to a diameter of  $D = 118(p/0.05)^{-0.5}$  km (where albedo  $p = 0.05$ ), or an  $H$ -magnitude of about 8.5. The “break” seen in the DES power law for Classical objects, at  $H = 7.2$ , is actually better explained as a limiting magnitude issue, with the DES survey efficiency likely being mis-estimated at the faintest, most difficult to detect magnitudes. Future work will explore the exact nature of the efficiency at faint magnitudes. For the time being, the DES data is only fit to  $H \leq 7.2$  (Classical) or  $H \leq 7.5$  (3:2 and Scattered) to avoid including the fainter magnitude data.

To test the hypothesis that the limiting magnitude was causing an artificial turnover, we tightened our discovery magnitude threshold from  $VR = 23$  to  $VR = 22.5$ . The same slope was found for the power law, but the “turnover” in the Classical population appeared at  $H \leq 6.7$  instead.

That said, there is one population that clearly samples the size distribution after the break in slope: the Centaurs. With 7 objects spanning a large range of  $H$ -magnitudes ( $7.5 < H < 11$ ), the Centaurs are well fit by a single, shallower power law, with  $\alpha = 0.44 \pm 0.04$ . (We note that similar slopes can be fit to the few Classical and 3:2 objects with  $H > 7.2$ , though they are strongly subject to the exact choice of the artificial break point and have a much smaller lever arm of 0.5-1 magnitudes.)

One model for the size distribution of the Kuiper Belt is to assume that brighter objects follow the Classical  $H$  magnitude distribution, and then there is a shift for smaller objects to the Centaur power law. Combining the bright slope fit to Classical objects with  $H \leq 7.2$  with the faint slope fit to Centaurs with  $H \geq 7.5$ , we can construct a double power law:  $\alpha_1 = 0.989 \pm 0.011$ ,  $\alpha_2 = 0.44 \pm 0.04$ , and  $H_b = 7.2$  (see Table 3). Note that this break point may well be an artifact of the limiting magnitudes of our fields, as very few objects (esp. Classical) were found at fainter than  $M > 23$ , and so our CDFs suffer from incompleteness.

We check the compatibility of each of the eight classes of KBOs with this double power law using a Kolmogorov-Smirnov (KS) test, with one additional variable: although the values for  $\alpha_1$ ,  $\alpha_2$ , and  $H_b$  are kept the same, the absolute number of objects is allowed to vary. The reasoning behind this choice is that objects in a resonance may have the same overall size distribution, but due to efficiencies of resonance capture may differ in absolute abundance. At the 5% level, all eight classes are compatible with this double power law. The scaling constants required, relative to the number of Classical objects,  $N_C = 2.6 * 10^{-4}$ , are as follows:  $N_{Scattered} = N_C$ ,  $N_{3:2} = 0.25N_C$ ,  $N_{2:1} = 0.15N_C$ ,  $N_{5:2} = 0.15N_C$ ,  $N_{7:4} = 0.03N_C$  and  $N_{5:3} = 0.03N_C$ . The Centaurs are much less populous, with an approximate scale of  $N_{Centaur} \sim 0.005N_C$ . Figure 1 shows the fit for the Classical population scaled by the appropriate scale factor for each class.

With an absolute scale and both slopes, we can estimate the total number of objects in each class less than a particular  $H$ -magnitude. Table 4 shows the estimated total number of objects in each class from  $H = 4 - 9$ , under two assumptions: (1) that  $\alpha_1$  applies throughout the whole  $H$  range (as would be the case if the break at  $H = 7.2$  is an instrumental magnitude effect and the true break is around objects of 100 km diameter; see the literature discussion in Section 6.3); and (2) that the break at  $H = 7.2$  is real. The errors are calculated by taking the difference between the number calculated using the nominal power law and using  $\pm 1 \sigma$  error. Note that the Centaurs are estimated using their own independent fit and errors.

#### 4.2.2. Estimating class distribution parameters

To fully characterize a class of objects, more than just a size distribution is required. Objects in a dynamical class can be defined by distribution functions of their orbital properties, which may be approximated by simple functional forms ([e.g., a Lorentzian to describe the inclination distribution, as in G10]).

A second approach to estimating class populations is to use a maximum-likelihood method of determining the best model parameters of the distribution functions for the parameters ( $a$ ,  $e$ ,  $i$ , and  $H$ ) that define the class. These distributions can then be used to calculate the detected fraction,  $f$ , from Equation 26, to find the total number of objects within our parameter range. A downside to maximum likelihood is that more objects are needed in a class to full characterize the four-dimensional parameter space. Only the Classical, Scattered, and 3:2 classes have sufficient objects to attempt a ML fit, and the Scattered fit is marginal. This is why we recommend the values derived from the CDFs in Section 4.2.1 for comparison between many classes of objects.

We used somewhat expanded subsets of objects for the Scattered and 3:2 classes compared to the CDF analysis. For the ML analyses, a well-sampled parameter space is important, and we examined cutoffs for  $H$ -magnitude from  $H = 6.5 - 8.5$ . The addition of a few fainter objects tends to decrease the fitted value for  $\alpha$  ( $\alpha_C = 0.99 \pm 0.09$  if we fit objects with  $H \leq 7.0$  cutoff but  $\alpha_C = 0.60 \pm 0.06$  for  $H \leq 7.5$ ), but has little effect on the parameters for the  $a$ ,  $e$ , and  $i$  distributions. Choosing a lower cutoff means decreasing the sample size, and since there were few enough objects to start with, the cutoff was set at  $H = 7.5$  for the Scattered and 3:2 classes. Classical objects are fit to the previously determined CDF cutoff of  $H = 7.2$ .

For all three classes we chose to model the  $a$ ,  $e$ , and  $i$  distributions using a single Lorentzian (Equation 16), following the preference for Lorentzians over Gaussians of E05 and G10. The Classical inclination distribution is also well fit by a double Gaussian (as in G10), but since the resulting distributions are not meaningfully different, the simpler model is preferred in this work. The distributions and histograms of the biased and de-biased detections are shown in Figure 3 (Classical), Figure 4 (3:2), and Figure 5 (Scattered).

We list the best fit values for the Classical, 3:2, and Scattered distributions in Table 5. The values for  $\alpha$  agree within their errors with the slopes found for the Classical objects in the CDF analysis. The distributions were normalized over the observed range of parameters for  $a$  and  $H$ <sup>1</sup>, and from  $0 \leq e \leq 0.95$  and  $0 \leq i \leq 170^\circ$  (the full range has been truncated to avoid numerical errors near boundaries). We note that the the eccentricity distribution for the Scattered objects is artificially narrow due to a small number of low-probability objects at  $e = 0.18$  (an effect that would presumably go away with more objects).

Using the calculated distribution functions, we evaluate Equation 26 along a grid of 4-7 points each in  $a$ - $e$ - $i$ - $H$  space to find the detected fraction,  $f$ . The grid was constructed assuming that each grid object was discovered at its median distance from the sun (i.e., half its time is spent closer to the sun, and half its time is further out) and with the discovery magnitude calculated for that distance using the value of  $H$  from the grid:

$$m_d = H + 5 \log_{10}(R_d/1) + 5 \log_{10}(R_d - 1/1). \quad (33)$$

For the Classical objects,  $f_{Classical} = 0.026$  for  $H \leq 7.2$ . The fraction for 3:2 objects is three times smaller,  $f_{3:2} = 0.0097$ , while the fraction of Scattered objects detected is over ten times smaller, with  $f_{Scattered} = 0.002$  (both for  $H \leq 7.5$ ).

---

<sup>1</sup>Minimum/maximum values for Classical objects:  $37.2 \leq a \leq 50.3$  AU and  $4.7 \leq H \leq 7.2$ ; Scattered objects:  $32.5 \leq a \leq 68.1$  AU and  $5.3 \leq H \leq 7.3$ ; 3:2 objects:  $39 \leq a \leq 40$  AU and  $4.7 \leq H \leq 7.4$ ;

The corresponding total number of objects estimated (by maximizing Equation 28 for  $N'_o$ ) is found to be  $N_{<7.2} = 4800 \pm 430$  Classical objects,  $N_{<7.5} = 3300 \pm 580$  3:2 objects, and  $N_{<7.5} = 12,000 \pm 2400$  Scattered objects. We can compare both the total number of objects and the ratios to those found with the CDF fits (see Tables 5 and 4). For *ratios*, the ML approach yields ratios in agreement with the CDF ratios: for every Classical object there are 0.35 objects in the 3:2 resonance (compared to 0.25 from CDFs) and 1.2 Scattered objects (compared to 1). The *absolute* number of objects found using ML is larger than in the CDF fits, perhaps because the same probabilities are used to infer missing objects along more dimensions. For objects with  $H \leq 7$ , the estimate from ML is 1.3 times as large for Classical objects, 1.9 times as large for 3:2 objects, and 1.7 times as large for Scattered objects.

## 5. Comparison to other observations

### 5.1. CFEPS

There are three ways in which the two largest surveys differ in observations and analysis, which should be considered when comparing results.

1. *Differences in observational strategies.* The specific strategies used have been described in detail elsewhere (Millis et al. 2002; Elliot et al. 2005; Petit et al. 2011; Gladman et al. 2012), and may affect populations of observed and recovered objects. Both teams have tailored their de-biasing calculations to address their object *discovery bias* (the subject of this paper).

One area of potential concern relates to the *recovery bias*. The DES found a much larger number of objects initially, but due to limited telescope resources was unable to track and classify all of them, resulting in a smaller percentage recovered and classified compared to CFEPS. The breakdown of which types of DES objects were lost after initial discovery was reported in Elliot et al. (2005), and lost objects tended to be fainter (requiring better follow-up conditions) and faster-moving (allowing for less time to recover an object before errors accumulated) than objects that were successfully tracked. Future work will explore how important the recovery bias is. We note that the advent of all-sky surveys like PAN-STARRS and LSST will mean that many of these objects will eventually be recovered and linked back to the original observations with high quality orbits due to the long observational baselines, mitigating any current recovery bias.

2. *Differences in class definitions.* Although mean-motion resonances are straightforward to identify, the precise meaning of a “Classical” or “Scattered” object differs somewhat

between groups. For large groups of objects such as the Classicals, such a difference only affects a few objects at the margins and is unlikely to have a large impact on the overall conclusions. Smaller groups, however, such as the CFEPS Scattering population (11 objects, Shankman et al. 2013), draws members from what the DES would classify as Scattered and Centaur groups. Given the low numbers of objects in most classes, it is possible that these definitions will make a difference in the overall class definitions, and care should be taken when comparing results.

3. *Differences in statistical approach.* The DES approach is a forward-modeling method, where we calculate the biases of discovering each object at a randomized point in its orbit, and turn that into a discovery probability. Two methods are used to extrapolate from individual probabilities to class populations. The  $H$ -magnitude CDF method has each known object stand in for the  $(1 / \text{probability})$  objects that we didn't find with similar parameters. The ML method fits for distributions of  $H$ - $a$ - $e$ - $i$ , assuming functional forms such as power laws or Lorentzians, for each class. Although the ML method results in larger absolute numbers, it produces results consistent with the CDF fits at the 1-2  $\sigma$  level. Given the inability to use the ML method for most dynamical classes, we use the CDF results to compare with the size distributions found by other groups.

By contrast, CFEPS follows a backward-modeling approach, making synthetic populations of objects (drawn from distribution functions for  $H$ - $a$ - $e$ - $i$  as well as orbital longitude and libration amplitude for resonant objects). These synthetic populations are run through the CFEPS Survey Simulator to find which ones would have been detected. The properties of the initial distributions are adjusted until they match the recovered populations.

A full and complete comparison of these two methods would apply both methods to both surveys, and is the subject of future work.

Despite the differences noted above, the CFEPS and DES results do agree on the power law *slopes* for most classes. We find the Classical objects have  $\alpha_C = 0.989 \pm 0.011$ , which is consistent with the independently derived 3:2 slope of  $\alpha_{3:2} = 0.986 \pm 0.041$ . CFEPS, meanwhile, has carved the main belt into several sections (hot, stirred, and kernel), with slopes of 0.8, 1.2, and 1.2 respectively (Petit et al. 2011); when combined together, as in Figure 1, the CFEPS distribution is similar in slope to the DES result.

The *absolute numbers* of CFEPS objects are generally the same order of magnitude as the DES results, but not entirely consistent. The Classical numbers reported by Petit et al. (2011) must be scaled upward by a factor of 1.4 to be consistent with the absolute number of DES objects (at the 5% level using a KS test). The largest resonant class, the 3:2 objects, are consistent if the CFEPS numbers of Gladman et al. (2012) are scaled upward by 1.3.

By contrast, the Scattered objects are not within the same order of magnitude: to reach 5% consistency with a KS test, they must be scaled upward by a factor of 16 from the values reported in Petit et al. (2011).

The ratios between classes also sometimes differ between the two surveys. The DES finds 4 times as many Classical as 3:2 objects, while CFEPS finds 8 times as many. Other resonances agree: both the 5:3 and 7:4 classes have similar slopes and absolute numbers (as shown in Figure 1). (Note that the 5:3 and 7:4 both have few objects, with 5 and 10 DES discoveries and 6 and 5 CFEPS discoveries, respectively.) Future work is needed to resolve the apparent discrepancies.

## 5.2. Hot and Cold Classical populations

Once individual object probabilities have been calculated, we can divide the DES sample into classes to meet any categorization scheme proposed in the literature. Recent work by Fraser et al. (2010) examined the Kuiper Belt by subdividing it into “Hot”, “Cold” and “Close” populations. No distinction is made between dynamical class, instead dividing the sample into objects discovered between  $38 \leq R \leq 48$  and  $i < 4$  (“Cold”);  $30 \leq R \leq 150$  and  $4 < i < 90$  (“Hot”); and  $30 \leq R \leq 38$  and  $4 < i < 90$  (“Close”). We examined the DES sample using the same criteria (plus our restriction to objects with  $M \leq 23$ ) and found that the best-fit slopes were  $\alpha_{Hot} = 0.94 \pm 0.03$ ,  $\alpha_{Cold} = 1.36 \pm 0.02$ , and  $\alpha_{Close} = 1.07 \pm 0.08$ . These numbers are very similar to recent work by Fraser, despite using completely different objects and de-biasing methods ( $\alpha_{Cold} = 1.46$  with a break at  $H = 6.9$ , and  $\alpha_{Hot} = 0.93$  with a break at  $H = 7.1$ , presented at the 2012 DPS meeting and private communication).

## 5.3. One-in-a-million (and rarer) objects

By necessity, the least probable objects – for instance, those with very distant semi-major axes that have high eccentricities – have generally been excluded from this analysis. We found that including a few such objects that were widely scattered in semi-major-axis space led to huge distortions in the resulting distributions derived for all of the parameters. Hence, our Scattered class was cut to include only objects with  $a \leq 80$  AU. We excluded 9 objects that otherwise met our selection criteria ( $m_d \leq 23$  and quality 3 orbits), with  $82 \leq a \leq 653$  AU, classified various as Scattered-Near, Scattered-Extended, and Centaurs depending on their other dynamical properties.

All of these objects are highly unlikely to be observed based largely on their eccentricity,

but not enough of them are known to define a class of their own. The least-probable object with  $M_d \leq 23$ , the Centaur 87269, has a discovery probability of  $4 * 10^{-8}$  due to its extreme average distance from the Sun ( $a = 653$  AU and  $e = 0.97$ ) as well as its relatively high inclination ( $i = 19$ ). Taken at face value, these objects imply vast reserves of similar, undetected and undetectable far-flung objects. Turning a few rare detections into a quantitative estimate of the size and orbital parameter distributions of such objects is beyond the scope of this paper.

## 6. Comparison to theory

As Neptune migrated outward during the early history of the solar system, it captured objects in the primordial disk into mean-motion resonances and carried them with it. In principle, we can use the relative number of objects in different classes to distinguish between different models for how Neptune migrated, because objects in different orbits are captured with varying efficiency. For instance, one model that considers the effect of gaseous drag on objects has the 3:2 resonance favored to capture many more objects than the 2:1 resonance (Jiang and Yeh 2004). Using the de-biased detection results of the previous sections, the DES finds about half as many objects in the 2:1 as in the 3:2 resonance. We now examine several models of planet formation and see how they compare to the DES class populations.

### 6.1. Smooth migration

Other models of the outer solar system include a smooth model of migration. In particular, Hahn and Malhotra (2005) numerically simulated the relative numbers of objects in different classes, allowing for more direct comparison with the data. This model assumes that the giant planets migrated smoothly outwards and always kept small eccentricities, and focused on the overall structure of the resultant Kuiper Belt after migration finished, including relative proportions of different dynamical classes.

A major conclusion of Hahn and Malhotra (2005) is that Neptune migrated into a dynamically hot disk, that is, a disk in which the small bodies had already been stirred up to significant eccentricities and inclinations. The numerical model for migration into a cold disk ( $\langle e \rangle = 0.001$  and  $\langle \sin i \rangle = \langle e \rangle / 2$ ) could not create objects with the same range of high inclinations that we observe among known KBOs. However, if the initial disk had previously been excited by some other, unspecified mechanism, so that  $\langle e \rangle = 0.1$ , then the final model inclination range is in good agreement with the observed inclination distribution.

If the initial disk were dynamically hot, the prediction is that higher-order resonances would be much more efficient at capturing objects than if the disk were cold. The 5:2 resonance, which is a relatively strong resonance, would collect a substantial number of objects, but so would a number of distant and high-order resonances which would not be populated at all if Neptune migrated through a cold disk. DES objects have been found in 7 of the 10 “exotic” resonances cited by Hahn and Malhotra (2005), including the 11:6, 9:4, 7:3, 12:5, 3:1, 7:2, and 4:1 (Table 1).

We can also directly compare the numbers of objects in the Centaurs, Main Belt (Classicals), Scattered Disk, and 3:2 and 2:1 resonances. Table 1 in Hahn and Malhotra (2005) lists the number of objects from 50-1000 km in radius, or approximately  $H = 9.0$  using their assumed albedo of 0.04. We can compare their values to the DES values in Table 4. If we assume that the power law breaks at  $H_b = 7.2$ , we find ( $N_{H \leq 9}$ ): 80 vs. 110 DES Centaur; 130,000 vs. 21,000 DES Classical; 25,000 vs. 21,000 DES Scattered; 5300 vs. 3200 DES 2:1; and 2700 vs. 5300 DES 3:2 objects. In absolute numbers, most DES class numbers are within a factor of 2 of the values from Hahn and Malhotra (2005), with a few important caveats: (1) the number of Classical objects is strongly overestimated by Hahn and Malhotra (2005); (2) the relative ratio of 2:1 objects to 3:2 objects is reversed, with Hahn and Malhotra (2005) predicting twice as many 2:1 objects when we find the opposite, and (3) the absolute and relative number of Classical and Scattered objects also differ (we find equal numbers, where their model predicts five times as many Classicals).

Other problems were noted in their paper, such as the inability to explain objects with  $i > 15$  degrees or to populate the extended scattered disk (perihelia beyond 40 AU), where objects such as Sedna and several DES objects have been found. For all of these reasons, smooth migration cannot fully explain the evolution of the outer solar system.

## 6.2. Nice Model

An important recent model of planetary migration in the outer solar system, the “Nice Model” (Gomes et al. 2005; Tsiganis et al. 2005; Levison et al. 2008), examines the effects of Jupiter and Saturn crossing a mutual 2:1 resonance. This model is used to explain the Late Heavy Bombardment of Earth and the Moon as the result of a sharp increase in the eccentricities of the giant planets, which scatters objects in the Kuiper and asteroid belts inward.

In general, the Nice Model is more successful than previous attempts at explaining Kuiper Belt structure. The inclination distribution of the Classical objects is bi-modal



(Gulbis et al. 2010), which the Nice Model can reproduce. The semi-major axis and eccentricity distributions modeled also match observations. Other predictions from Levison et al. (2008) include the eccentricity and inclination distribution of the 3:2 resonance, where it was noted that the observations tend to have higher eccentricities than the simulations, and observational bias was suggested to explain the difference. In fact, Figure 4 shows the de-biased 3:2 eccentricity distribution to be even more eccentric. We similarly confirm that the problem noted with the eccentricities of the Classical belt being smaller than produced in simulation still persists after de-biasing.

### 6.3. Location of the power law break

There has long been evidence that the size distribution of Kuiper Belt objects cannot follow a single power law. A break in the size distribution power law has been proposed for objects smaller than about 100 km diameter (Gladman et al. 2001; Bernstein et al. 2004). Destructive collisions have been evoked to explain the existence of a break at roughly the same size (e.g., 40 km Pan and Sari 2005). The exact location of the size break, however, has not yet been observed because of the faint magnitudes of objects in this size regime: 100 km with an albedo of 0.05 roughly corresponds to  $H = 9$ .

Collisional evolution modeling by Fraser (2009) presents theoretical support for a depletion region from  $D = 20–40$  km, with reduced collision rates for larger objects ( $D = 50–100$  km), allowing the steep power law from the brighter Kuiper Belt to continue until that point. A “divot” is expected in the power law at around that point. Recently, there has been a claimed detection of that “divot” around  $H = 9$  (Shankman et al. 2013), based on 11 Scattering objects discovered and de-biased by CFEPS using their Survey Simulator. These objects range in brightness from  $H = 7.1–10$ , with only two objects (L4k09 and L4v11) fainter than the supposed “divot” point ( $H = 9.5$  and  $H = 10.0$ , respectively).

The only class observed by the DES with objects fainter than about  $H = 8.5$  is the Centaurs, which approach closer than Neptune and are consequently often much brighter at discovery. Although Centaurs are now located inside the inner edge of the Kuiper Belt, they are thought to be the transitional stage between the scattered disk and Jupiter family comets (JFCs). This is supported by both dynamical evolution calculations (Levison and Duncan 1997; Tiscareno and Malhotra 2003) and the similarity of the Centaur inclination distribution (Gulbis et al. 2010) to both the Scattered objects and JFCs (and not to the main Kuiper Belt or resonant objects).

The slope observed for the Centaur objects,  $\alpha_2 = 0.44 \pm 0.04$ , is consistent with other

populations of small objects reported in the literature, such as the Jupiter Family Comets ( $\alpha = 0.49 \pm 0.05$ , Solontoi et al. 2012). It is also the same power law as the Jupiter Trojans ( $\alpha = 0.44 \pm 0.05$ , Solontoi et al. 2012). We find no evidence of a break in the Centaur size distribution, with 7 objects between  $H = 7.5 - 11$  and  $m_d \leq 23$  discovered by the DES (Figure 6). Most of our objects are fainter than the purported “divot” point found by Shankman et al. (2013). No sign of turnover is seen out to  $H = 11$  ( $D = 40$  km assuming albedo=0.05).

Recent models by Schlichting and Sari (2011) and Schlichting et al. (2013) predict that large KBOs ( $R \geq 50$  km) follow a power law of the form  $N \sim R^q$ , with  $q = 4$ . This model (Figure 1 of Schlichting et al. 2013) agrees with the overall *shape* of the power law derived from the DES observations, but the *scale* of the model is about three times larger than we observed. Even accounting for the relative class abundances, the Schlichting model finds a factor of 3 times as many objects the DES data. Figure 7 shows the DES data plotted on top of the model predictions from Schlichting et al. (2013), where the DES observations in Figure 7 are scaled up by a factor of 3 (Classical), 12 (3:2), and 600 (Centaur). (Note that the ratio between the classes is the same as the ratio between classes in Table 4, with an overall factor of 3 times greater abundance in the model.)

As noted by Schlichting et al. (2013), a de-biased population of Centaurs has been needed to probe the critical range of small objects, with diameters from 1-100 km. The DES sample covers much of this range (down to  $H = 11$ , or 37.5 km diameter if the albedo=0.05 and smaller for higher albedos). The transition in the observed Centaur objects occurs smoothly with no need for a divot. KS tests for each class reveal that all classes are consistent at the 95% level with the Schlichting model, if they are scaled up from their DES abundances by a factor of 3.

An additional feature of the Schlichting et al. (2013) model is a turnover at large sizes, roughly  $R = 500 - 1000$  km. This is seen in the 3:2 objects, where a few large objects with  $H \leq 5$  ( $R = 300$  km for the same albedo of 0.05) follow a shallower slope than other objects ( $\alpha_{H < 5} = 0.17 \pm 0.04$ ). The model, however, predicted a steeper slope. With only two detections, though, it is difficult to conclude anything except that small number statistics apply.

## 7. Conclusions

The Kuiper Belt contains a record of outer solar system history, and de-biased observations of different classes of objects are a powerful tool to understanding it. The DES is

the largest uniform survey to weigh in on the dynamical statistics. Here we have presented an analysis of a dataset of 304 objects, as well as a new method for accounting for discovery biases.

We have calculated the detection probability for 304 objects with secure orbital classifications, accounting for biases related to the object semi-major axis, eccentricity, inclination, discovery magnitude, discovery distance, and absolute magnitude. Using these probabilities, we can estimate the size distribution for 246 objects in 8 classes with at least 5 objects each, using  $H$ -magnitude as an observable proxy for object diameter. The population of Classical objects is used to derive the main power law slope,  $\alpha_1$ , and the fainter/smaller Centaur population to derive the slope after the break point,  $\alpha_2$ , we derive a broken power law that is consistent with all eight classes for which we have sufficient objects. The parameters of this power law are  $\alpha_1 = 0.989 \pm 0.011$  for  $H \leq 7.2$  and  $\alpha_2 = 0.44 \pm 0.04$  for fainter objects, with the location of the physical break still uncertain. It is unclear whether the break in our data is an artifact of incomplete magnitude correction at the faint end, which we plan to pursue further with the revised magnitude calibration in a later paper. For that reason, results are shown for both a single power law and a double power law out to  $H = 9$ .

We note that this power law also appears to break down at the very brightest, and largest, objects ( $H < 5$ ), as is seen in the 3:2 distribution. This may be due to small number statistics in the objects detected, the stochastic nature of a few large-body collisions, or a change in the underlying mechanisms that govern the formation of large objects.

We can also estimate the total number of objects in the Kuiper Belt up to a particular size range. Two different methods were used, a max-likelihood estimation that determined distribution functions for four quantities ( $a, e, i, H$ ) and a CDF based directly on inverted probabilities that only determined the  $H$  magnitude distribution. For comparison between classes, we prefer the CDF results, which were possible on 8 classes (maximum likelihood only worked on three). We note that the ratios between the classes are similar in the max-likelihood analysis, although the overall abundances of objects are 1.5-2 times larger. We adopt the CDF as our estimates, and find that for  $H \leq 7$  the number of objects in 8 classes: Classical ( $2200 \pm 400$  objects), Scattered ( $2200 \pm 400$ ), 3:2 ( $550 \pm 100$ ), 2:1 ( $330 \pm 60$ ), 5:2 ( $550 \pm 100$ ), 7:4 ( $66 \pm 12$ ), 5:3 ( $66 \pm 12$ ), and Centaur ( $15 \pm 4$ ).

Finally, we can compare our data to other reported observations and model predictions. The absolute number and power law slope agree with results presented by another large survey, CFEPS, for the Classical objects. Some additional classes of objects (such as the 5:3 and 7:4 resonances) also agree. Others, notably the 3:2 resonance, differ in absolute numbers by a factor of 2 and in ratio to the Classical objects by a factor of 4. These discrepancies in the details illustrate the value of having two completely independent data sets and analyses

methods to determine the number of objects in the Kuiper Belt. Future work is planned to explain the differences between the two surveys and to arrive at a consensus value.

The model by Schlichting et al. (2013) agrees well with our data except for the brightest ( $H < 5$ ) objects, of which we have very few. Other models predict break points in size ranges that are not well-sampled by our data, but the Centaur population agrees with the slopes found for small objects (less than 100 km diameter or fainter than roughly  $H = 9$ ). We find no evidence for the divot reported in Shankman et al. (2013). Dividing our sample according to the “Hot”, “Cold”, and “Close” criteria of Fraser et al. (2010), we found excellent agreement in reported power law slopes.

In anticipation of large all-sky surveys such as PAN-STARRS and LSST, we are making this de-biasing code available<sup>2</sup> so that the discovery probabilities of objects found by any survey with the same characterizations can be calculated. We anticipate this will be a useful complement to tools such as the CFEPS Survey Simulator for determining the structure of the Kuiper Belt.

This research was supported in part by NASA Grants NAG5-13380, NAG5-11058, and NNG06-GI23G to Lowell Observatory; NSF Grants AST0406493 and AST0707609 to MIT; the Alfred P. Sloan Foundation at UCB, and NASA Grant nos. NAG5-4495 and NAG5-12236 at UH. DET acknowledges support from the American Astronomical Society in the form of a Small Research Grant and from the Space Telescope Science Institute under grant GO-9433.06. Support for program GO-9433 was provided by NASA, through a grant from the Space Telescope Science Institute, which is operated by the Association of Universities for Research in Astronomy (AURA), Inc. under NASA contract NAS 5-26555. NOAO distributes the IRAF program, used for some of the image processing in this paper, and NOAO maintains the observing facilities used in this investigation. NOAO is operated by AURA, under cooperative agreement with the National Science Foundation. A. Gulbis specifically acknowledges support by the National Research Foundation of South Africa. S. Benecchi acknowledges support through a Carnegie Fellowship at the Department of Terrestrial Magnetism.

---

<sup>2</sup><https://github.com/elisabethadams/des-class-populations>

## REFERENCES

- Bernstein, G. M., Trilling, D. E., Allen, R. L., Brown, M. E., Holman, M., and Malhotra, R.: 2004, *AJ* **128**, 1364
- Bevington, P. R. and Robinson, D. K.: 2003, *Data reduction and error analysis for the physical sciences*
- Bottke, W. F., Vokrouhlický, D., Minton, D., Nesvorný, D., Morbidelli, A., Brassier, R., Simonson, B., and Levison, H. F.: 2012, *Nature* **485**, 78
- Brown, M. E.: 2001, *AJ* **121**, 2804
- Buie, M. W., Trilling, D. E., Wasserman, L. H., and Crudo, R. A.: 2011, *ApJS* **194**, 40
- Crooke, P., Froeb, L., and Tschantz, S.: 1999, *Mathematica in Education and Research* **8(1)**, 17
- Elliot, J. L., Kern, S. D., Clancy, K. B., Gulbis, A. A. S., Millis, R. L., Buie, M. W., Wasserman, L. H., Chiang, E. I., Jordan, A. B., Trilling, D. E., and Meech, K. J.: 2005, *AJ* **129**, 1117
- Fraser, W. C.: 2009, *ApJ* **706**, 119
- Fraser, W. C., Brown, M. E., and Schwamb, M. E.: 2010, *Icarus* **210**, 944
- Fraser, W. C. and Kavelaars, J. J.: 2008, *Icarus* **198**, 452
- Fuentes, C. I. and Holman, M. J.: 2008, *AJ* **136**, 83
- Gladman, B., Kavelaars, J. J., Petit, J.-M., Morbidelli, A., Holman, M. J., and Loredó, T.: 2001, *AJ* **122**, 1051
- Gladman, B., Lawler, S. M., Petit, J.-M., Kavelaars, J., Jones, R. L., Parker, J. W., Van Laerhoven, C., Nicholson, P., Rousselot, P., Bieryla, A., and Ashby, M. L. N.: 2012, *AJ* **144**, 23
- Gladman, B., Marsden, B. G., and Vanlaerhoven, C.: 2008, *Nomenclature in the Outer Solar System*, pp 43–57
- Gomes, R., Levison, H. F., Tsiganis, K., and Morbidelli, A.: 2005, *Nature* **435**, 466
- Grav, T., Jedicke, R., Denneau, L., Chesley, S., Holman, M. J., and Spahr, T. B.: 2011, *PASP* **123**, 423

- Gulbis, A. A. S., Elliot, J. L., Adams, E. R., Benecchi, S. D., Buie, M. W., Trilling, D. E., and Wasserman, L. H.: 2010, *AJ* **140**, 350
- Gulbis, A. A. S., Elliot, J. L., and Kane, J. F.: 2006, *Icarus* **183**, 168
- Hahn, J. M. and Malhotra, R.: 2005, *AJ* **130**, 2392
- Ivezic, Z., Tyson, J. A., Acosta, E., Allsman, R., Anderson, S. F., Andrew, J., Angel, R., Axelrod, T., Barr, J. D., Becker, A. C., Becla, J., Beldica, C., Blandford, R. D., Bloom, J. S., Borne, K., Brandt, W. N., Brown, M. E., Bullock, J. S., Burke, D. L., Chandrasekharan, S., Chesley, S., Claver, C. F., Connolly, A., Cook, K. H., Cooray, A., Covey, K. R., Cribbs, C., Cutri, R., Daues, G., Delgado, F., Ferguson, H., Gawiser, E., Geary, J. C., Gee, P., Geha, M., Gibson, R. R., Gilmore, D. K., Gressler, W. J., Hogan, C., Huffer, M. E., Jacoby, S. H., Jain, B., Jernigan, J. G., Jones, R. L., Juric, M., Kahn, S. M., Kalirai, J. S., Kantor, J. P., Kessler, R., Kirkby, D., Knox, L., Krabbendam, V. L., Krughoff, S., Kulkarni, S., Lambert, R., Levine, D., Liang, M., Lim, K., Lupton, R. H., Marshall, P., Marshall, S., May, M., Miller, M., Mills, D. J., Monet, D. G., Neill, D. R., Nordby, M., O'Connor, P., Oliver, J., Olivier, S. S., Olsen, K., Owen, R. E., Peterson, J. R., Petry, C. E., Pierfederici, F., Pietrowicz, S., Pike, R., Pinto, P. A., Plante, R., Radeka, V., Rasmussen, A., Ridgway, S. T., Rosing, W., Saha, A., Schalk, T. L., Schindler, R. H., Schneider, D. P., Schumacher, G., Sebag, J., Seppala, L. G., Shipsey, I., Silvestri, N., Smith, J. A., Smith, R. C., Strauss, M. A., Stubbs, C. W., Sweeney, D., Szalay, A., Thaler, J. J., Vanden Berk, D., Walkowicz, L., Warner, M., Willman, B., Wittman, D., Wolff, S. C., Wood-Vasey, W. M., Yoachim, P., Zhan, H., and for the LSST Collaboration: 2008, *ArXiv e-prints*
- Jewitt, D. and Luu, J.: 1993, *Nature* **362**, 730
- Jewitt, D., Luu, J., and Trujillo, C.: 1998, *AJ* **115**, 2125
- Jiang, I.-G. and Yeh, L.-C.: 2004, *MNRAS* **355**, L29
- Levison, H. F. and Duncan, M. J.: 1997, *Icarus* **127**, 13
- Levison, H. F., Morbidelli, A., Vanlaerhoven, C., Gomes, R., and Tsiganis, K.: 2008, *Icarus* **196**, 258
- Lykawka, P. S. and Mukai, T.: 2007, *Icarus* **189**, 213
- Malhotra, R.: 1993, *Icarus* **106**, 264
- Millis, R. L., Buie, M. W., Wasserman, L. H., Elliot, J. L., Kern, S. D., and Wagner, R. M.: 2002, *AJ* **123**, 2083

- Morbidelli, A., Levison, H. F., Bottke, W. F., Dones, L., and Nesvorný, D.: 2009, *Icarus* **202**, 310
- Morbidelli, A., Levison, H. F., and Gomes, R.: 2008, *The Dynamical Structure of the Kuiper Belt and Its Primordial Origin*, pp 275–292
- Morbidelli, A., Levison, H. F., Tsiganis, K., and Gomes, R.: 2005, *Nature* **435**, 462
- Noll, K. S., Grundy, W. M., Schlichting, H. E., Murray-Clay, R. A., and Benecchi, S. D.: 2012, in *AAS/Division for Planetary Sciences Meeting Abstracts*, Vol. 44 of *AAS/Division for Planetary Sciences Meeting Abstracts*, p. 405.07
- Pan, M. and Sari, R.: 2005, *Icarus* **173**, 342
- Petit, J.-M., Kavelaars, J. J., Gladman, B. J., Jones, R. L., Parker, J. W., Van Laerhoven, C., Nicholson, P., Mars, G., Rousselot, P., Mousis, O., Marsden, B., Bieryla, A., Taylor, M., Ashby, M. L. N., Benavidez, P., Campo Bagatin, A., and Bernabeu, G.: 2011, *AJ* **142**, 131
- Schlichting, H. E., Fuentes, C. I., and Trilling, D. E.: 2013, *ArXiv e-prints*
- Schlichting, H. E. and Sari, R.: 2011, *ApJ* **728**, 68
- Shankman, C., Gladman, B. J., Kaib, N., Kavelaars, J. J., and Petit, J. M.: 2013, *ApJ* **764**, L2
- Sheppard, S. S.: 2012, *AJ* **144**, 169
- Solontoi, M., Ivezić, Ž., Jurić, M., Becker, A. C., Jones, L., West, A. A., Kent, S., Lupton, R. H., Claire, M., Knapp, G. R., Quinn, T., Gunn, J. E., and Schneider, D. P.: 2012, *Icarus* **218**, 571
- Stansberry, J., Grundy, W., Brown, M., Cruikshank, D., Spencer, J., Trilling, D., and Margot, J.-L.: 2008, *Physical Properties of Kuiper Belt and Centaur Objects: Constraints from the Spitzer Space Telescope*, pp 161–179
- Thirouin, A., Ortiz, J. L., Duffard, R., Santos-Sanz, P., Aceituno, F. J., and Morales, N.: 2010, *A&A* **522**, A93
- Tiscareno, M. S. and Malhotra, R.: 2003, *AJ* **126**, 3122
- Trujillo, C. A., Jewitt, D. C., and Luu, J. X.: 2001, *AJ* **122**, 457
- Tsiganis, K., Gomes, R., Morbidelli, A., and Levison, H. F.: 2005, *Nature* **435**, 459

Walsh, K. J., Morbidelli, A., Raymond, S. N., O’Brien, D. P., and Mandell, A. M.: 2012,  
*Meteoritics and Planetary Science* p. 214



Table 1. Objects per class

Class	All $Q = 3^a$	... also $m_d \leq 23$	... also $H \leq 7.5$	... also $H \leq 7.2$
1:1	1	1	1	0
2:1	7	6	5	5
3:1	1	1	0	0
3:2	51	49	33	27
4:1	1	1	1	1
4:3	3	3	1	1
5:2	7	6	6	3
5:3	5	5	3	2
5:4	3	3	3	2
7:2	1	0	0	0
7:3	3	3	2	0
7:4	11	10	9	8
9:4	3	3	3	3
9:5	2	1	1	1
11:6	1	1	1	1
12:5	1	1	1	1
Classical	144	130	129	122
Centaur <sup>b</sup>	8	7	1	0
Scattered <sup>c</sup>	41	33	24	22
Far <sup>d</sup>	10	9	7	6
Total	304	273	231	205

<sup>a</sup>Secure orbital classifications (quality 3) only.

<sup>b</sup>The Centaur class in this analysis is restricted to dynamical Centaurs with  $a \leq a_{Nep}$ .

<sup>c</sup>The Scattered class in this analysis is restricted to dynamical Centaurs, Scattered-Near or Scattered Extended objects with  $a_{Nep} < a \leq 80$  AU.

<sup>d</sup>Far objects are dynamical Centaurs, Scattered-Near or Scattered Extended objects with  $a > 80$  AU.

Table 2. Detection probability for DES objects with secure classifications

Object	Class	$a$ (AU)	$e$	$i$ (deg)	$H$	$m_d$ (VR)	$R_d$ (AU)	Prob. <sup>a</sup>	Fit <sup>b</sup>
2001QR322	1:1	30.38	0.0297	1.3438	7.42	21.1	29.654	0.25	
2001FQ185	2:1	47.471	0.2258	2.2422	7.01	23.2	36.985	0.000091	
2003FE128	2:1	47.714	0.2487	3.2774	6.17	21.5	36.019	0.017	
2001UP18	2:1	48.008	0.0702	0.43497	5.71	22.5	50.271	0.062	
2000QL251	2:1	48.043	0.2192	4.7652	6.54	22.2	38.211	0.0081	
2002VD130	2:1+4:2I	48.096	0.3272	3.3745	7.11	21.9	33.445	0.011	
2004TV357	2:1	48.128	0.2827	11.155	6.63	21.6	36.839	0.011	
2004VK78	2:1	48.207	0.3358	0.7672	8.16	22.4	32.549	0.0035	
136120	3:1	61.837	0.4756	21.383	7.9	22.3	32.838	0.00017	
119069	3:2	39.022	0.2404	1.8456	7.1	22.6	37.156	0.044	Y
169071	3:2	39.094	0.1888	7.1794	8.	24.5	34.69	0.000021	
2005GV210	3:2	39.143	0.1727	11.806	6.75	22.8	40.774	0.013	Y
2002GE32	3:2	39.164	0.2294	16.259	7.13	22.9	40.06	0.0076	Y
2002GF32	3:2	39.166	0.178	2.213	5.69	21.	42.181	0.32	Y
2005GE187	3:2	39.208	0.3233	18.837	7.3	22.1	31.849	0.0059	Y
2002CE251	3:2	39.231	0.2656	10.039	8.38	22.6	29.956	0.0014	
2003FL127	3:2	39.236	0.2374	4.8246	6.17	22.4	47.025	0.12	Y
2002GW31	3:2	39.265	0.244	3.8494	6.94	22.6	40.07	0.057	Y
2001KY76	3:2	39.277	0.237	2.4311	6.09	21.5	39.057	0.21	Y
2005GF187	3:2	39.287	0.252	2.7169	7.84	22.6	31.131	0.0089	
2005GB187	3:2	39.288	0.2331	15.558	7.04	21.6	30.156	0.0086	Y
2002GY32	3:2	39.298	0.0863	3.0394	6.87	21.5	35.978	0.16	Y
2004EH96	3:2	39.302	0.2781	4.3025	8.13	21.9	28.56	0.013	
2002GL32	3:2	39.324	0.1229	7.1363	7.85	22.6	34.495	0.0048	
2002GV32	3:2	39.335	0.1886	3.9293	7.4	21.3	32.459	0.1	Y
307463	3:2	39.339	0.2068	2.9165	6.1	21.4	43.01	0.23	Y
2003FF128	3:2	39.355	0.2122	0.3827	6.71	21.6	33.082	0.069	Y
2004EV95	3:2	39.359	0.1871	12.544	7.4	23.3	41.424	0.0048	
2003QB91	3:2	39.385	0.1898	5.3942	6.1	21.7	44.671	0.16	Y
2004EJ96	3:2	39.401	0.237	9.1549	7.86	23.	33.743	0.0018	

Table 2—Continued

Object	Class	$a$ (AU)	$e$	$i$ (deg)	$H$	$m_d$ (VR)	$R_d$ (AU)	Prob. <sup>a</sup>	Fit <sup>b</sup>
2005EZ300	3:2	39.411	0.237	10.708	7.28	22.4	35.426	0.0089	Y
306792	3:2	39.413	0.1559	17.038	7.2	21.7	36.772	0.024	Y
28978	3:2	39.42	0.2458	18.278	3.3	19.	43.344	0.057	
133067	3:2	39.422	0.2565	9.6145	6.8	21.5	32.127	0.025	Y
2000CK105	3:2	39.435	0.2317	9.2204	6.1	22.7	48.436	0.051	Y
2001KD77	3:2	39.437	0.1115	1.5235	5.62	20.5	35.27	0.27	Y
2001KB77	3:2	39.44	0.2806	18.514	7.25	21.7	31.665	0.0087	Y
2003QX111	3:2	39.464	0.1308	8.8664	6.59	21.5	39.314	0.078	Y
2003QH91	3:2	39.468	0.1483	5.2109	6.65	22.	41.727	0.11	Y
2001QF298	3:2	39.499	0.1069	21.777	4.73	20.	42.579	0.049	Y
69990	3:2	39.501	0.1907	7.8294	8.3	22.4	32.646	0.0052	
91205	3:2	39.507	0.1356	11.591	8.	22.7	35.236	0.0027	
2001RX143	3:2	39.51	0.2938	18.89	6.11	22.1	40.504	0.019	Y
1998WV31	3:2	39.523	0.2728	4.5887	8.28	22.4	32.916	0.017	
2004VT75	3:2	39.54	0.2112	12.373	6.26	21.5	36.495	0.036	Y
2002CW224	3:2	39.548	0.2431	6.0052	6.93	22.3	39.025	0.047	Y
2003UT292	3:2	39.556	0.299	18.213	6.93	21.1	30.936	0.016	Y
2001QH298	3:2	39.568	0.1089	5.4677	7.67	22.	36.576	0.05	
2003UV292	3:2	39.59	0.218	12.168	7.22	22.2	33.906	0.0083	Y
2003WA191	3:2	39.604	0.2404	4.5802	8.5	22.1	30.237	0.011	
2001RU143	3:2	39.612	0.1444	7.236	5.98	22.2	43.831	0.077	Y
139775	3:2	39.616	0.1982	6.0159	7.2	20.1	32.11	0.15	Y
1998WS31	3:2	39.661	0.2064	6.6648	8.25	22.6	31.51	0.0025	
2004VZ75	3:2	39.694	0.1913	4.2463	7.3	22.6	42.14	0.061	Y
69986	3:2	39.707	0.2292	15.089	7.9	22.3	31.282	0.0024	
2002VD138	3:2	39.746	0.1505	4.12	8.44	22.8	34.886	0.0058	
1998WZ31	3:2	39.758	0.1725	13.549	8.11	22.7	33.022	0.0012	
1998UR43	3:2	39.78	0.2262	7.68	8.34	22.4	31.935	0.0049	
2002VX130	3:2	39.79	0.2285	2.8342	8.35	22.1	30.811	0.019	
119473	3:2	39.971	0.292	3.1909	7.1	22.4	32.506	0.015	Y

Table 2—Continued

Object	Class	$a$ (AU)	$e$	$i$ (deg)	$H$	$m_d$ (VR)	$R_d$ (AU)	Prob. <sup>a</sup>	Fit <sup>b</sup>
2003LA7	4:1	75.796	0.5269	5.1198	6.13	21.8	45.58	0.0077	
2005ER318	4:3	36.495	0.1606	11.352	7.72	22.1	31.417	0.01	
1998UU43	4:3	36.682	0.1289	10.709	6.79	22.8	37.784	0.012	
2004TX357	4:3	36.853	0.2165	15.522	8.55	22.6	29.361	0.00095	
119068	5:2	54.856	0.3544	11.751	6.7	21.5	35.418	0.0045	
135571	5:2+5:2I	55.041	0.3489	14.012	7.2	22.3	38.189	0.0016	
2002GP32	5:2	55.098	0.4189	0.73692	6.99	20.3	32.163	0.064	
2004EG96	5:2	55.248	0.4198	16.569	8.01	23.1	32.222	0.000039	
38084	5:2	55.305	0.4113	12.703	7.4	22.	35.355	0.0023	
69988	5:2	55.543	0.4291	9.191	7.4	22.6	38.614	0.0023	
2004TT357	5:2	56.026	0.438	10.095	7.44	22.2	31.511	0.00072	
2002GS32	5:3	42.043	0.1054	5.8249	7.45	22.2	37.642	0.02	
2000QN251	5:3	42.419	0.1282	1.3872	7.2	22.4	37.006	0.015	
143751	5:3+5:3I	42.515	0.2583	7.1891	8.6	22.6	31.536	0.0015	
149349	5:3	42.57	0.2425	8.102	6.8	22.	40.042	0.024	
2002VV130	5:3	42.647	0.1749	2.4766	7.51	22.7	37.151	0.01	
127871	5:4	34.895	0.0862	1.0169	7.	21.6	32.714	0.17	
2002GW32	5:4	34.906	0.0775	7.926	7.18	21.6	37.603	0.1	
2003QB92	5:4	34.956	0.0901	2.151	7.24	22.2	37.35	0.2	
160148	7:2	69.147	0.5034	14.555	7.8	23.3	39.194	0.000067	
95625	7:3	52.81	0.3732	13.462	7.4	21.2	33.289	0.0055	
183964	7:3	53.08	0.3831	9.7465	7.4	22.5	33.7	0.00075	
2002CZ248	7:3	53.207	0.3919	4.355	8.27	22.9	35.314	0.0011	
1999HG12	7:4	43.443	0.1537	1.4773	7.18	22.5	43.109	0.053	
135024	7:4	43.502	0.1123	1.7254	6.8	23.	45.805	0.037	
119070	7:4	43.517	0.1723	3.2705	7.	21.6	36.02	0.062	
119066	7:4	43.537	0.0788	5.8422	6.8	22.2	42.698	0.044	
118378	7:4	43.577	0.1111	3.5257	7.4	23.3	41.634	0.0028	
119956	7:4	43.768	0.1724	2.5205	6.1	21.	42.004	0.23	
2000OP67	7:4	43.787	0.1882	1.6823	7.27	22.5	38.776	0.028	

Table 2—Continued

Object	Class	$a$ (AU)	$e$	$i$ (deg)	$H$	$m_d$ (VR)	$R_d$ (AU)	Prob. <sup>a</sup>	Fit <sup>b</sup>
2003QW111	7:4	43.879	0.1138	1.485	6.44	21.4	45.068	0.25	
2003QX91	7:4+7:4I	43.892	0.2535	28.088	8.22	22.7	33.107	0.0003	
2004PW107	7:4	43.964	0.1368	3.483	6.55	21.3	38.875	0.13	
2001QE298	7:4	43.966	0.1603	3.946	6.8	21.7	37.71	0.065	
2001KG76	9:4	51.34	0.3397	0.021179	6.43	21.9	43.869	0.15	
182397	9:4	51.756	0.233	15.954	5.9	22.5	46.134	0.0052	
42301	9:4	51.871	0.2825	2.262	4.2	20.5	48.744	0.31	
2002GD32	9:5	44.349	0.1406	6.3612	5.95	21.5	50.194	0.15	
2001KL76	9:5	44.361	0.1006	2.8444	6.47	23.1	48.389	0.042	
182294	11:6	44.812	0.1593	9.7814	6.6	22.3	38.541	0.0058	
119878	12:5	53.982	0.3477	16.948	6.1	21.1	35.903	0.0077	
54598	CENTAURR	16.564	0.2007	21.525	7.5	19.7	19.486	0.042	Y
2003QD112	CENTAURR	19.089	0.5809	14.73	10.74	20.4	11.458	0.009	Y
2003QC112	CENTAURR	20.553	0.2731	17.552	8.48	21.7	25.776	0.043	Y
2003UY292	CENTAURR	22.023	0.2776	8.1602	10.22	21.9	15.909	0.0061	Y
2000CO104	CENTAURR	24.057	0.1461	3.751	10.08	22.8	20.646	0.0041	Y
119976	CENTAURR	24.103	0.3884	3.7289	11.	22.2	14.998	0.0034	Y
2002PQ152	CENTAURR	25.891	0.1904	10.448	8.74	20.8	21.095	0.047	Y
88269	CENTAURR	25.912	0.2369	4.4225	9.5	23.4	22.414	0.0014	
120181	CENTAURR	32.566	0.178	2.0828	7.3	20.6	27.142	0.19	Y <sup>c</sup>
2004TE282	CENTAURR	34.65	0.1596	19.694	8.25	22.6	32.246	0.0038	<sup>c</sup>
87555	CENTAURR	34.985	0.5622	7.8098	8.3	20.5	18.116	0.01	<sup>c</sup>
149560	CENTAURR	41.617	0.4764	33.54	8.1	20.5	24.372	0.0039	<sup>c</sup>
2005EB299	CENTAURR	51.99	0.5106	1.8756	8.13	22.3	25.874	0.0014	<sup>c</sup>
127546	CENTAURR	66.796	0.6858	76.346	8.	20.6	21.973	0.00021	<sup>c</sup>
2003FH129	CENTAURR	71.318	0.6134	18.374	8.27	23.1	33.931	0.000088	<sup>c</sup>
2005PU21	CENTAURR	180.63	0.838	6.5096	6.32	22.	49.206	0.00042	
87269	CENTAURS	652.78	0.9682	19.004	9.2	22.2	21.795	$4.1 \times 10^{-8}$	
135182	CLASSICAL	37.24	0.0184	3.0487	6.2	22.	36.885	0.12	Y
2003FD128	CLASSICAL	38.166	0.0202	4.5304	7.26	23.2	37.555	0.0047	

Table 2—Continued

Object	Class	$a$ (AU)	$e$	$i$ (deg)	$H$	$m_d$ (VR)	$R_d$ (AU)	Prob. <sup>a</sup>	Fit <sup>b</sup>
2003QA92	CLASSICAL	38.331	0.0621	1.9449	6.65	20.7	37.83	0.27	Y
82157	CLASSICAL	38.506	0.0575	4.632	6.9	23.5	38.98	0.0029	
2003QQ91	CLASSICAL	38.968	0.0734	4.2853	7.47	22.1	39.344	0.091	
1998WV24	CLASSICAL	39.201	0.0403	2.1148	7.14	22.5	38.224	0.041	Y
80806	CLASSICAL	42.187	0.0687	3.0332	6.7	21.9	41.658	0.13	Y
88268	CLASSICAL	42.362	0.0165	0.43869	6.3	21.6	42.252	0.16	Y
2005JZ174	CLASSICAL	42.457	0.075	5.3707	6.52	21.6	42.492	0.13	Y
2003FK127	CLASSICAL	42.492	0.0465	0.82101	7.18	22.7	40.793	0.019	Y
2002CD251	CLASSICAL	42.547	0.0141	1.223	7.16	22.9	42.512	0.021	Y
2003QG91	CLASSICAL	42.607	0.0205	2.1091	7.27	22.8	42.325	0.023	
2002VT130	CLASSICAL	42.683	0.0318	2.3887	5.77	21.5	42.653	0.19	Y
2003QN91	CLASSICAL	42.718	0.1122	4.2729	7.22	21.6	38.031	0.083	
2001QB298	CLASSICAL	42.744	0.0967	3.3341	6.91	21.4	39.037	0.14	Y
69987	CLASSICAL	42.761	0.0245	1.0048	7.2	22.8	42.019	0.017	Y
2005JP179	CLASSICAL	42.783	0.0265	1.3795	5.86	20.7	42.16	0.25	Y
1999HV11	CLASSICAL	42.784	0.0287	2.8516	7.78	22.8	43.578	0.031	
88267	CLASSICAL	42.836	0.025	1.0938	7.2	22.5	42.944	0.059	Y
2003QY90	CLASSICAL	42.847	0.0503	2.2327	6.48	21.7	45.	0.22	Y
2003UN284	CLASSICAL	42.871	0.009	2.6743	7.42	23.2	42.486	0.006	
1999HJ12	CLASSICAL	42.883	0.0467	3.2114	7.32	22.6	44.188	0.05	
134860	CLASSICAL	42.948	0.019	0.446	6.1	21.7	42.612	0.15	Y
2004DM71	CLASSICAL	43.008	0.033	0.79791	7.16	22.5	43.853	0.066	Y
2003UT291	CLASSICAL	43.028	0.0554	1.2279	6.33	22.5	45.068	0.099	Y
2000CL105	CLASSICAL	43.03	0.0458	2.7209	6.34	22.2	44.999	0.12	Y
2002CS154	CLASSICAL	43.062	0.0457	0.44797	7.18	22.5	42.237	0.034	Y
2004UD10	CLASSICAL	43.095	0.0311	2.551	6.46	22.5	44.132	0.057	Y
2001FK185	CLASSICAL	43.105	0.0366	1.0018	7.38	25.7	41.721	$7.6 \times 10^{-7}$	
2001QO297	CLASSICAL	43.11	0.0385	1.1344	5.81	22.4	43.528	0.083	Y
2003QE91	CLASSICAL	43.131	0.0496	3.6187	7.07	22.7	41.222	0.0063	Y
2000ON67	CLASSICAL	43.138	0.0266	2.151	6.03	22.6	44.274	0.056	Y

Table 2—Continued

Object	Class	$a$ (AU)	$e$	$i$ (deg)	$H$	$m_d$ (VR)	$R_d$ (AU)	Prob. <sup>a</sup>	Fit <sup>b</sup>
2003QF91	CLASSICAL	43.138	0.0391	1.3088	7.17	22.4	41.882	0.054	Y
160256	CLASSICAL	43.14	0.0598	3.3646	6.3	21.8	45.366	0.17	Y
2003QE112	CLASSICAL	43.163	0.0441	2.6719	6.5	21.6	44.863	0.19	Y
2003QL91	CLASSICAL	43.165	0.013	1.7288	6.62	21.9	42.72	0.17	Y
2003QZ111	CLASSICAL	43.18	0.0642	3.8618	6.76	22.	40.415	0.065	Y
2000OU69	CLASSICAL	43.222	0.0493	2.9953	6.21	22.1	41.132	0.077	Y
2001RW143	CLASSICAL	43.282	0.0385	1.9022	7.14	22.9	41.622	0.012	Y
2002VB131	CLASSICAL	43.339	0.0356	0.26848	6.25	22.6	44.679	0.044	Y
2002CZ154	CLASSICAL	43.349	0.0577	9.3039	7.4	22.7	40.881	0.0055	
2002PD155	CLASSICAL	43.398	0.0104	6.9551	6.79	22.8	43.061	0.011	Y
2003QD91	CLASSICAL	43.4	0.0341	0.83966	6.84	22.2	41.993	0.069	Y
1999HH12	CLASSICAL	43.41	0.022	2.8173	7.02	22.6	44.081	0.048	Y
2005EM303	CLASSICAL	43.413	0.0173	4.1308	7.47	23.1	42.758	0.0067	
1998WY24	CLASSICAL	43.414	0.044	0.39369	6.58	22.3	41.856	0.037	Y
119067	CLASSICAL	43.431	0.1902	6.4212	6.6	21.9	44.138	0.075	Y
129772	CLASSICAL	43.511	0.0309	1.8241	7.2	22.6	42.245	0.035	Y
2003QY111	CLASSICAL	43.526	0.0387	1.3893	6.71	22.1	42.107	0.087	Y
1998WX24	CLASSICAL	43.558	0.0359	0.97684	6.57	22.8	45.12	0.031	Y
2004PX107	CLASSICAL	43.595	0.053	1.892	7.04	23.	41.468	0.0081	Y
2003FM127	CLASSICAL	43.607	0.0614	3.3609	6.77	22.8	43.243	0.021	Y
2003QU90	CLASSICAL	43.645	0.0582	3.0919	7.15	22.4	43.072	0.054	Y
2005EC318	CLASSICAL	43.725	0.0368	1.0643	6.24	22.4	44.309	0.077	Y
2002CU154	CLASSICAL	43.741	0.0593	1.8545	6.74	22.6	41.174	0.025	Y
2003QX90	CLASSICAL	43.833	0.0209	2.1281	6.68	21.8	44.685	0.18	Y
2002PQ145	CLASSICAL	43.855	0.0475	2.9071	5.51	20.7	45.877	0.26	Y
2005GX186	CLASSICAL	43.859	0.0154	3.3568	6.65	23.6	43.442	0.0016	
2001FK193	CLASSICAL	43.876	0.0657	1.9738	6.86	23.8	42.598	0.00076	
275809	CLASSICAL	43.884	0.0809	0.32597	5.6	20.2	42.546	0.2	Y
2003QF113	CLASSICAL	43.907	0.0302	3.0095	6.55	22.1	42.587	0.088	Y
53311	CLASSICAL	43.912	0.0607	1.3276	6.6	22.6	43.841	0.044	Y



Table 2—Continued

Object	Class	$a$ (AU)	$e$	$i$ (deg)	$H$	$m_d$ (VR)	$R_d$ (AU)	Prob. <sup>a</sup>	Fit <sup>b</sup>
2004VU75	CLASSICAL	43.923	0.1328	2.4578	6.55	22.4	41.889	0.05	Y
2000CF105	CLASSICAL	43.927	0.0391	1.2035	6.82	22.8	42.243	0.017	Y
2000CN114	CLASSICAL	43.929	0.0447	0.386	7.19	22.	44.084	0.09	Y
2004OL12	CLASSICAL	43.938	0.0675	2.3867	6.12	22.3	43.624	0.085	Y
2005GC187	CLASSICAL	43.938	0.1223	2.9635	7.02	22.7	38.674	0.0085	Y
1999HS11	CLASSICAL	43.945	0.0174	1.0874	6.54	22.5	43.775	0.054	Y
2001DD106	CLASSICAL	43.958	0.0947	0.82671	6.86	23.	40.619	0.0051	Y
2002CB225	CLASSICAL	43.963	0.0776	2.2267	7.19	22.6	42.019	0.029	Y
2004EU95	CLASSICAL	43.983	0.0392	1.6911	6.71	22.8	42.26	0.016	Y
2005EF298	CLASSICAL	43.984	0.0883	1.522	6.05	21.4	41.025	0.16	Y
307616	CLASSICAL	43.997	0.0777	10.156	5.4	19.9	44.485	0.086	Y
2005EX297	CLASSICAL	44.006	0.1102	4.4748	6.11	23.1	45.317	0.014	
2000CE105	CLASSICAL	44.011	0.0597	1.0616	6.82	23.	41.383	0.0061	Y
2001FL185	CLASSICAL	44.039	0.0745	2.1814	7.12	23.5	40.889	0.0012	
2003QV90	CLASSICAL	44.061	0.0551	1.6099	6.95	22.1	43.899	0.11	Y
2002XH91	CLASSICAL	44.067	0.0851	3.5128	5.52	21.5	47.69	0.21	Y
2002FX36	CLASSICAL	44.095	0.0516	2.6337	6.28	22.2	45.661	0.11	Y
2000CJ105	CLASSICAL	44.108	0.1095	10.843	5.86	21.9	47.533	0.055	Y
88611	CLASSICAL	44.131	0.0243	4.0269	5.8	21.8	44.967	0.14	Y
2004PY107	CLASSICAL	44.169	0.0947	0.41522	6.24	21.4	41.055	0.13	Y
2002PO149	CLASSICAL	44.173	0.0598	0.99542	6.46	21.6	46.098	0.2	Y
2001QQ322	CLASSICAL	44.191	0.0557	2.5497	6.23	21.6	43.626	0.18	Y
2002CY154	CLASSICAL	44.196	0.077	0.77915	6.47	22.9	47.593	0.049	Y
2001QJ298	CLASSICAL	44.214	0.0409	2.0786	6.14	21.4	45.232	0.22	Y
2000CP104	CLASSICAL	44.215	0.0993	8.238	6.66	22.5	46.784	0.034	Y
60454	CLASSICAL	44.227	0.0832	2.5344	6.3	22.	44.004	0.12	Y
2001QS322	CLASSICAL	44.231	0.0428	1.6546	5.92	21.	42.342	0.26	Y
2001KF76	CLASSICAL	44.25	0.0255	2.4047	7.11	22.7	44.466	0.038	Y
183963	CLASSICAL	44.263	0.0996	0.91072	7.2	22.8	42.219	0.013	Y
2000OH67	CLASSICAL	44.266	0.0184	4.1841	6.47	22.4	43.561	0.044	Y

Table 2—Continued

Object	Class	$a$ (AU)	$e$	$i$ (deg)	$H$	$m_d$ (VR)	$R_d$ (AU)	Prob. <sup>a</sup>	Fit <sup>b</sup>
2001QX297	CLASSICAL	44.269	0.031	2.4712	6.38	22.1	43.615	0.11	Y
2003QB112	CLASSICAL	44.3	0.1111	11.241	7.43	21.8	39.719	0.023	
2004DN64	CLASSICAL	44.316	0.0521	1.0277	7.58	23.5	42.024	0.0012	
2001RZ143	CLASSICAL	44.343	0.0695	2.5973	6.01	22.2	41.463	0.051	Y
2001QZ297	CLASSICAL	44.351	0.0636	2.2219	6.98	22.6	41.863	0.024	Y
2002VF131	CLASSICAL	44.361	0.0425	1.7053	6.63	22.5	44.5	0.063	Y
2000CL104	CLASSICAL	44.387	0.0786	1.0955	6.1	22.	42.564	0.11	Y
2003QJ91	CLASSICAL	44.419	0.054	1.0266	6.48	22.5	44.925	0.057	Y
2003QT91	CLASSICAL	44.431	0.0902	1.4422	6.67	22.1	40.913	0.054	Y
2001UN18	CLASSICAL	44.494	0.0697	3.5001	6.46	22.3	46.351	0.098	Y
148780	CLASSICAL	44.495	0.0597	5.5508	5.7	22.2	45.101	0.07	Y
2001QR297	CLASSICAL	44.504	0.0291	4.3395	6.28	21.6	43.633	0.14	Y
2003QA91	CLASSICAL	44.505	0.0706	0.89682	5.5	21.	45.262	0.22	Y
2000CN105	CLASSICAL	44.506	0.0995	3.1799	4.89	21.4	45.692	0.19	Y
2001QQ297	CLASSICAL	44.6	0.0862	2.9425	6.68	22.	42.362	0.092	Y
2005EN302	CLASSICAL	44.687	0.0665	2.3497	6.97	23.3	47.443	0.015	
2004DM64	CLASSICAL	44.797	0.1296	3.3272	6.78	22.8	41.55	0.011	Y
1998WW31	CLASSICAL	44.906	0.0828	8.0429	6.16	22.	46.577	0.061	Y
2001KT76	CLASSICAL	44.929	0.0855	2.273	6.92	22.9	42.3	0.011	Y
184314	CLASSICAL	44.98	0.1375	6.1414	6.3	22.	42.409	0.05	Y
2002CZ224	CLASSICAL	45.002	0.063	0.85619	7.14	23.	47.627	0.026	Y
2004ES95	CLASSICAL	45.104	0.1355	3.0388	6.77	22.5	41.197	0.023	Y
2003UN292	CLASSICAL	45.221	0.1139	1.5537	7.34	23.3	41.13	0.0016	
160091	CLASSICAL	45.264	0.1089	3.2665	6.8	22.7	42.269	0.015	Y
2001OQ108	CLASSICAL	45.36	0.0125	1.3674	6.53	22.9	45.757	0.019	Y
149348	CLASSICAL	45.365	0.1252	4.5418	6.3	21.8	41.269	0.071	Y
2002VD131	CLASSICAL	45.384	0.0649	0.74774	6.58	21.9	43.304	0.13	Y
2003UZ291	CLASSICAL	45.399	0.1306	6.4194	6.8	22.7	48.022	0.033	Y
2003LB7	CLASSICAL	45.403	0.1282	1.682	6.68	21.4	40.089	0.15	Y
2003GF55	CLASSICAL	45.407	0.0616	5.5284	6.51	23.3	46.455	0.0055	

Table 2—Continued

Object	Class	$a$ (AU)	$e$	$i$ (deg)	$H$	$m_d$ (VR)	$R_d$ (AU)	Prob. <sup>a</sup>	Fit <sup>b</sup>
2001QP297	CLASSICAL	45.409	0.1177	0.41271	6.42	21.8	43.304	0.09	Y
1998WY31	CLASSICAL	45.43	0.1178	1.0825	6.96	22.8	45.303	0.03	Y
2005EO304	CLASSICAL	45.479	0.065	1.8596	6.28	22.5	43.622	0.041	Y
2003QO91	CLASSICAL	45.555	0.1356	6.0962	6.71	21.4	39.457	0.07	Y
1998WX31	CLASSICAL	45.707	0.1123	2.5532	6.59	22.3	40.66	0.027	Y
1998WG24	CLASSICAL	45.828	0.1308	0.71848	6.51	22.	41.318	0.081	Y
2001KH76	CLASSICAL	46.018	0.123	4.7767	6.47	22.	44.767	0.078	Y
19521	CLASSICAL	46.027	0.1081	11.003	4.8	20.2	42.464	0.076	Y
2000CQ114	CLASSICAL	46.051	0.1155	2.2981	6.59	22.4	45.05	0.065	Y
2002CY248	CLASSICAL	46.245	0.1435	8.4779	5.17	21.4	52.057	0.094	Y
2001FO185	CLASSICAL	46.298	0.1162	11.267	6.74	24.2	41.188	0.000018	
2003QS91	CLASSICAL	46.336	0.1449	4.3372	7.4	22.2	40.207	0.022	
2004DH64	CLASSICAL	46.456	0.0913	2.4868	6.08	22.2	50.066	0.15	Y
2003QR91	CLASSICAL	46.641	0.1828	5.0561	6.31	20.8	38.678	0.12	Y
2002CT154	CLASSICAL	46.702	0.1116	3.1504	7.14	22.8	41.766	0.0065	Y
2005JR179	CLASSICAL	46.704	0.1149	2.4388	5.83	22.	45.303	0.11	Y
138537	CLASSICAL	46.734	0.1437	5.1841	5.9	21.7	40.895	0.057	Y
126719	CLASSICAL	46.906	0.1898	2.3308	6.7	22.1	38.864	0.031	Y
2003LD9	CLASSICAL	47.071	0.1698	8.2553	6.57	22.	40.601	0.017	Y
2001KA77	CLASSICAL	47.289	0.0957	13.216	5.12	21.2	48.945	0.058	Y
2003UY291	CLASSICAL	49.592	0.1669	4.0743	7.18	22.8	42.758	0.005	Y
182933	CLASSICAL	50.24	0.2382	0.68281	6.4	21.4	42.354	0.13	Y
38083	SCATEXTD	38.89	0.1559	12.775	6.7	22.1	38.252	0.024	Y
2004PA112	SCATEXTD	39.093	0.1124	32.223	7.06	21.7	35.836	0.011	Y
2004PT107	SCATEXTD	40.643	0.0604	27.264	5.98	20.8	38.438	0.029	Y
2001FU185	SCATEXTD	41.406	0.1655	23.798	9.	25.3	34.555	$1.1 \times 10^{-7}$	
2002GH32	SCATEXTD	41.885	0.0914	27.646	5.37	20.8	42.556	0.031	Y
2005JA175	SCATEXTD	42.293	0.1098	15.32	5.72	21.	46.617	0.054	Y
2001FN185	SCATEXTD	42.369	0.0695	22.27	7.11	24.5	39.524	$5.1 \times 10^{-6}$	
2003QA112	SCATEXTD	42.795	0.1142	16.223	5.95	21.4	47.197	0.048	Y

Table 2—Continued

Object	Class	$a$ (AU)	$e$	$i$ (deg)	$H$	$m_d$ (VR)	$R_d$ (AU)	Prob. <sup>a</sup>	Fit <sup>b</sup>
2004DG77	SCATEXTD	43.689	0.1244	48.138	7.14	23.7	45.831	0.00029	
2001KO77	SCATEXTD	43.767	0.1434	22.118	7.68	22.4	37.887	0.0024	
182934	SCATEXTD	44.086	0.1092	12.989	5.4	20.5	42.751	0.063	Y
138628	SCATNEAR	44.997	0.2687	16.065	7.1	22.	35.027	0.0046	Y
118379	SCATEXTD	45.131	0.2333	14.211	7.6	22.3	39.156	0.0065	
2004PB108	SCATEXTD	45.292	0.112	19.243	6.45	21.9	43.72	0.019	Y
2001KE77	SCATEXTD	45.311	0.1823	22.3	7.19	23.	38.758	0.00045	Y
2004PZ107	SCATEXTD	45.721	0.1876	12.344	7.3	22.3	38.658	0.0051	Y
2001KW76	SCATEXTD	45.869	0.2149	9.2413	7.7	22.9	40.328	0.0027	
2002VF130	SCATEXTD	46.075	0.1197	20.967	7.15	22.6	42.368	0.0027	Y
2001QA298	SCATEXTD	46.301	0.1902	22.2	6.68	22.	38.643	0.0048	Y
181855	SCATEXTD	46.31	0.1879	27.769	7.2	22.7	38.915	0.00074	Y
2000CG105	SCATEXTD	46.358	0.0417	29.237	6.47	22.8	46.423	0.0027	Y
2002CX224	SCATEXTD	46.437	0.1318	15.968	5.99	22.8	48.728	0.009	Y
2001FT185	SCATEXTD	46.928	0.1002	19.326	7.74	24.6	43.043	$3.7 \times 10^{-6}$	
2000CO105	SCATEXTD	47.157	0.1482	20.614	5.92	22.5	49.289	0.01	Y
2003UB292	SCATEXTD	47.359	0.0493	18.719	5.97	22.5	49.673	0.013	Y
2004PS107	SCATEXTD	47.94	0.2354	23.408	7.59	23.4	37.297	0.000051	
2004OL14	SCATNEAR	48.878	0.3063	19.849	8.08	22.4	34.016	0.00061	
181874	SCATEXTD	52.492	0.2554	17.616	6.8	24.7	41.392	$1.2 \times 10^{-6}$	
2004OJ14	SCATEXTD	55.245	0.2887	20.944	6.37	22.4	44.224	0.0022	Y
2000CQ105	SCATEXTD	56.917	0.3909	18.405	5.93	21.8	50.912	0.012	Y
60458	SCATEXTD	59.395	0.4022	20.983	6.6	22.7	44.109	0.0012	Y
2001KG77	SCATNEAR	61.431	0.4474	16.918	8.06	23.1	34.939	0.000042	
134210	SCATEXTD	62.435	0.3972	7.7491	6.8	21.4	37.851	0.0068	Y
2003QK91	SCATEXTD	68.016	0.4347	5.5719	6.63	21.8	40.502	0.0061	Y
2004TF282	SCATNEAR	81.825	0.5185	24.326	6.08	21.9	39.431	0.00031	
2005EF304	SCATEXTD	85.899	0.5514	18.55	7.24	22.8	40.06	0.000046	
118702	SCATEXTD	99.268	0.6044	24.375	6.8	21.9	40.231	0.00017	
184212	SCATNEAR	109.54	0.6773	15.763	7.2	21.9	35.896	0.00012	

Table 2—Continued

Object	Class	$a$ (AU)	$e$	$i$ (deg)	$H$	$m_d$ (VR)	$R_d$ (AU)	Prob. <sup>a</sup>	Fit <sup>b</sup>
2002GB32	SCATNEAR	203.1	0.826	14.025	7.61	21.7	37.146	0.00003	
82158	SCATNEAR	213.16	0.8394	30.665	6.	22.3	34.342	$2.*10^{-6}$	
148209	SCATNEAR	225.59	0.8047	21.435	6.3	22.6	52.712	0.000016	
2003FH127	SCATNEAR	738.63	0.95	1.262	7.23	23.3	36.978	$2.5*10^{-8}$	

<sup>a</sup>Probability of detecting object with listed parameters and randomized ecliptic longitude.

<sup>b</sup>Object used to derive fits. Centaur and Classical objects were used to derive CDF fits, and Classical, 3:2 and Scattered classes were used for maximum likelihood fits.

<sup>c</sup>Centaur with  $a_{Nep} < a < 80$  AU were grouped with Scattered objects for fits and plots throughout this paper.

Table 3. CDF fits to power law slope

Parameter	Value	Range	Derived from
$\alpha_1$	$0.989 \pm 0.011$	$4.8 \leq H \leq 7.2$	Classical CDF
$\alpha_2$	$0.44 \pm 0.04$	$7.5 \leq H \leq 11$	Centaur CDF

Table 4. Estimated number of objects less than  $H$

$\leq H$	Classical	Scattered	3:2	2:1	5:2	7:4	5:3	Centaur
(1) single power law, $\alpha_1 = 0.989$								$\alpha_{Cen} = 0.44$
4	$2 \pm 1$	$2 \pm 1$	$1 \pm 0$	$0 \pm 0$	$1 \pm 0$	$0 \pm 0$	$0 \pm 0$	$1 \pm 0$
5	$23 \pm 3$	$23 \pm 3$	$6 \pm 0$	$3 \pm 1$	$6 \pm 0$	$1 \pm 0$	$1 \pm 0$	$2 \pm 1$
6	$220 \pm 40$	$220 \pm 40$	$56 \pm 9$	$34 \pm 5$	$56 \pm 9$	$7 \pm 1$	$7 \pm 1$	$5 \pm 5$
7	$2200 \pm 400$	$2200 \pm 400$	$550 \pm 100$	$330 \pm 60$	$550 \pm 100$	$66 \pm 12$	$66 \pm 12$	$15 \pm 14$
7.5	$6800 \pm 1400$	$6800 \pm 1400$	$1700 \pm 300$	$1000 \pm 200$	$1700 \pm 300$	$200 \pm 50$	$200 \pm 50$	$25 \pm 26$
8	$21000 \pm 5000$	$21000 \pm 5000$	$5300 \pm 1200$	$3200 \pm 700$	$5300 \pm 1200$	$640 \pm 140$	$640 \pm 140$	$41 \pm 47$
9	$210000 \pm 50000$	$210000 \pm 50000$	$52000 \pm 13000$	$31000 \pm 8000$	$52000 \pm 13000$	$6200 \pm 1600$	$6200 \pm 1600$	$110 \pm 160$
(2) double power law, $\alpha_1 = 0.989$ , $H_b = 7.2$ , $\alpha_2 = 0.44$								$\alpha_{Cen} = 0.44$
7.5	$4700 \pm 1000$	$4700 \pm 1000$	$1200 \pm 200$	$700 \pm 160$	$1200 \pm 200$	$140 \pm 30$	$140 \pm 30$	$25 \pm 26$
8	$7700 \pm 2300$	$7700 \pm 2300$	$1900 \pm 600$	$1200 \pm 300$	$1900 \pm 600$	$230 \pm 70$	$230 \pm 70$	$41 \pm 47$
9	$21000 \pm 9000$	$21000 \pm 9000$	$5300 \pm 2300$	$3200 \pm 1300$	$5300 \pm 2300$	$640 \pm 270$	$640 \pm 270$	$110 \pm 160$
scale	1.	1.	0.25	0.15	0.15	0.03	0.03	NA

Table 5. Maximum likelihood fitted distribution parameters<sup>a</sup>

Param	Classical <sup>b</sup>	3:2 <sup>c</sup>	Scattered <sup>d</sup>
$\alpha$	$1.03 \pm 0.07$	$1.01 \pm 0.14$	$1.04 \pm 0.19$
$a_o$	$43.96 \pm 0.1$	$39.36 \pm 0.05$	$45.82 \pm 0.26$
$a_s$	$0.62 \pm 0.09$	$0.2 \pm 0.08$	$0.76 \pm 0.29$
$e_o$	$0.06 \pm 0.01$	$0.24 \pm 0.01$	$0.18 \pm 0.01$
$e_s$	$0.05 \pm 0.01$	$0.03 \pm 0.01$	$0.01 \pm 0.$
$i_o$	$1.82 \pm 0.16$	$14.77 \pm 1.5$	$21.89 \pm 0.71$
$i_s$	$1.32 \pm 0.24$	$4.07 \pm 1.66$	$1.51 \pm 0.48$
$H \leq 7.$	(3000)	(1000)	(3600)
$H \leq 7.2$	$4800 \pm 430$	(1600)	(5800)
$H \leq 7.5$	(9700)	$3300 \pm 580$	$12000 \pm 2400$

<sup>a</sup>Values in parentheses were not directly fit.

<sup>b</sup>Objects fit: quality 3,  $m_d \leq 23$ , and  $H \leq 7.2$ .

<sup>c</sup>Objects fit: quality 3,  $m_d \leq 23$ , and  $4 \leq H \leq 7.5$ .

<sup>d</sup>Objects fit: quality 3,  $m_d \leq 23$ , and  $H \leq 7.5$ .

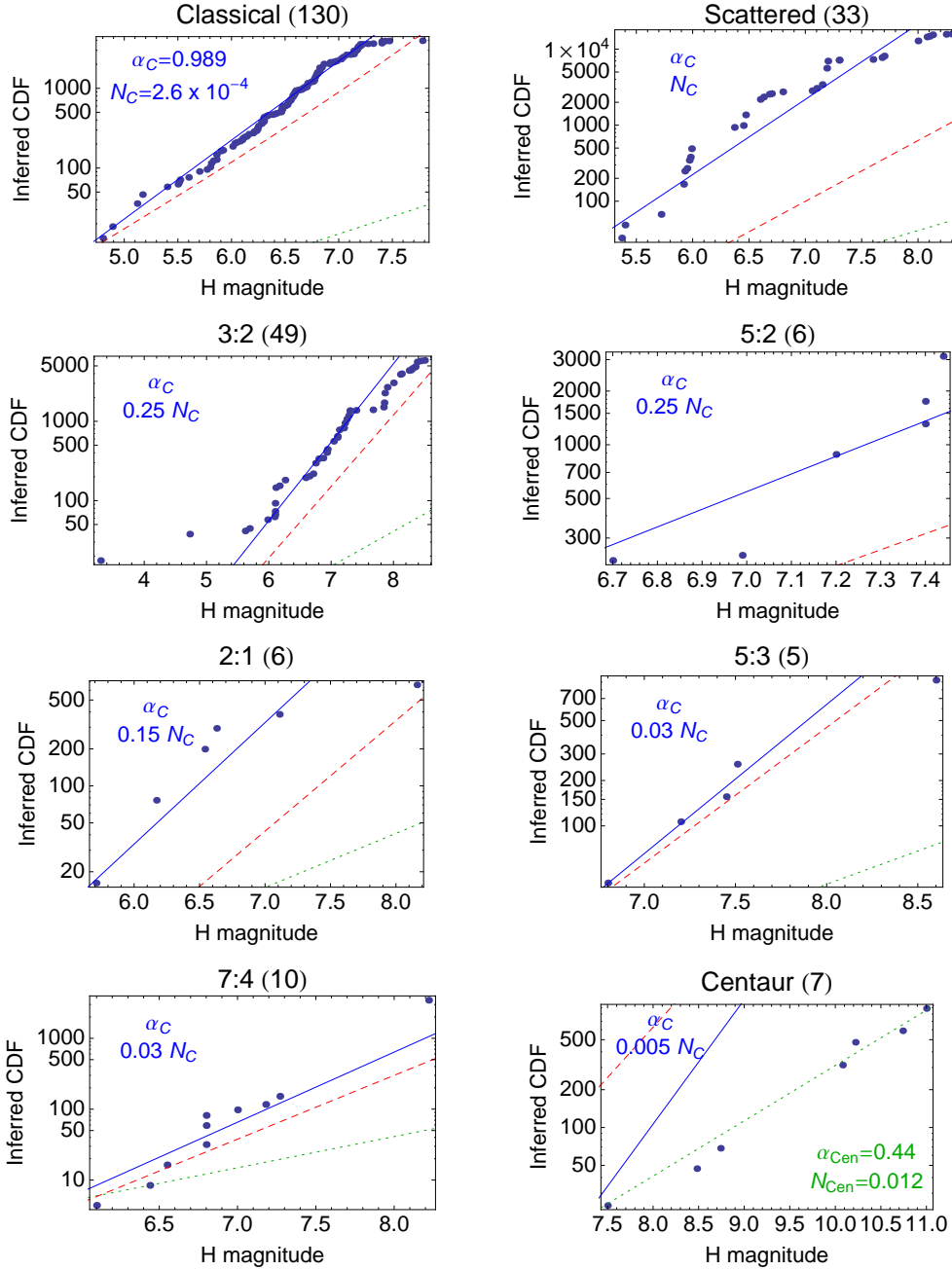


Fig. 1.— Cumulative distribution function by  $H$  magnitude for eight classes. The dots show the probability-weighted number of each DES object, based on Equation 30. The Classical distribution is fit between  $5 \leq H \leq 7.2$  with a slope of  $\alpha_C = 0.989 \pm 0.011$  and a scale factor of  $N_C = 2.6 * 10^{-4}$ . The blue line in each plot shows the same fit to the Classical, times a scale factor  $N_X$  that differs by class. Only the Centaurs are inconsistent with the Classical slope, and are independently fit to a shallower  $\alpha_{Cen} = 0.44 \pm 0.04$ ; this power law is plotted as a dotted green. For comparison, the dashed red lines show the power laws for each class derived by CFEPS (Gladman et al. 2012; Petit et al. 2011), with values for  $\alpha$  from 0.8 to 1.2. (Note that CFEPS did not provide a Centaur distribution; the Scattered distribution is shown for comparison.)



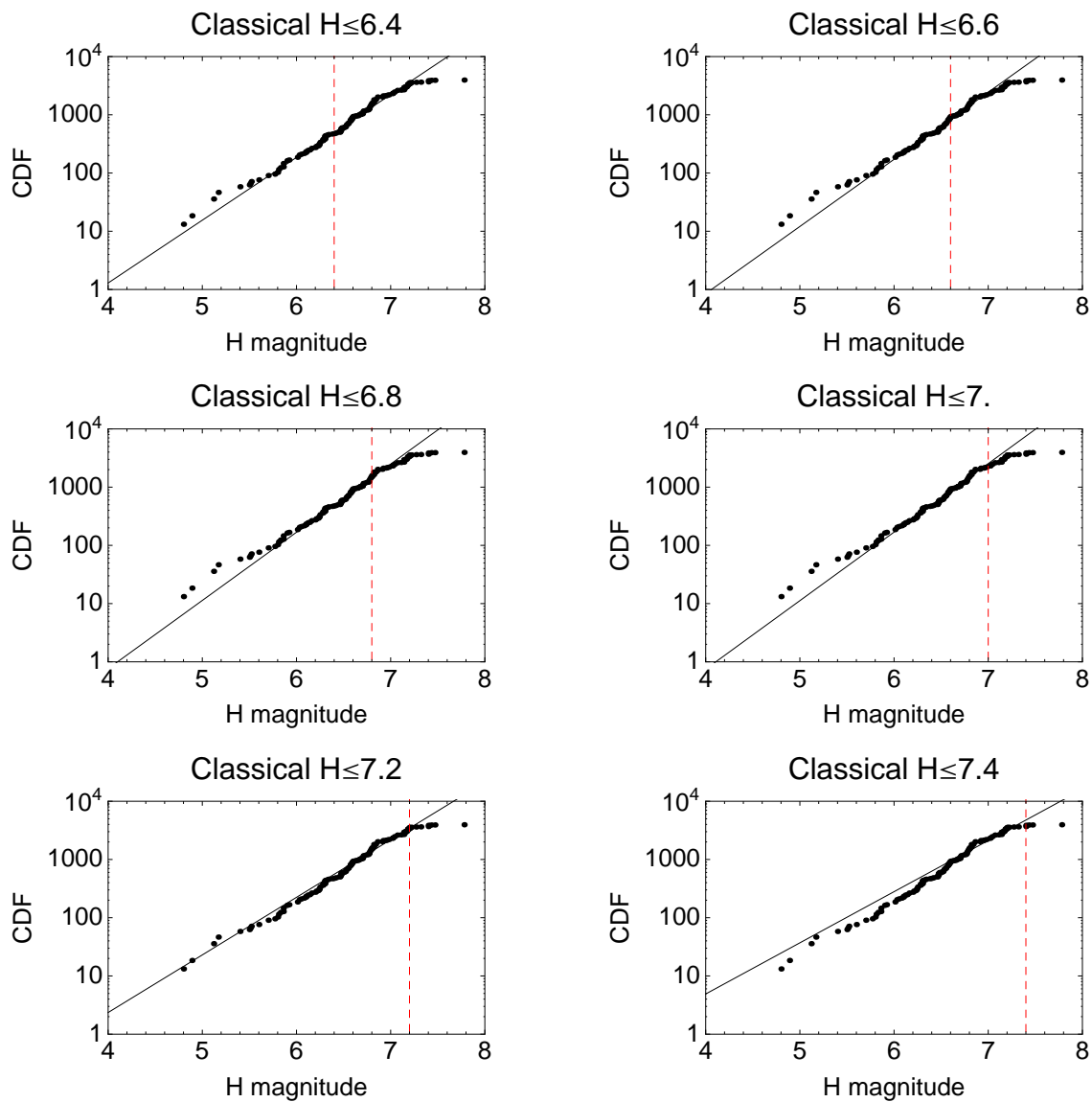


Fig. 2.— Determining the break point, using the Classical distribution. All objects brighter than the break point,  $H_b$  (dashed red line) are used to calculate the fit (solid line). The slope with the lowest error is derived when  $H_b = 7.2$ . This break may be due to limitations in the faint magnitude sensitivity and not a physical cause.

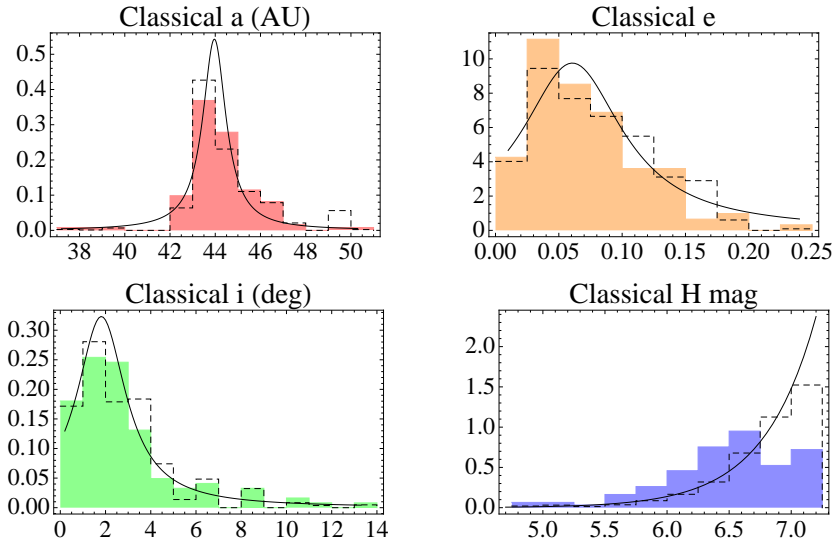


Fig. 3.— Maximum likelihood fit to 122 Classical objects with  $m_d \leq 23$ , and  $H \leq 7.2$ . The filled histogram shows the observed distribution, while the dashed histogram shows the amount by which the distribution is adjusted to account for discovery probabilities. The black lines show the best maximum likelihood fit to each parameter.

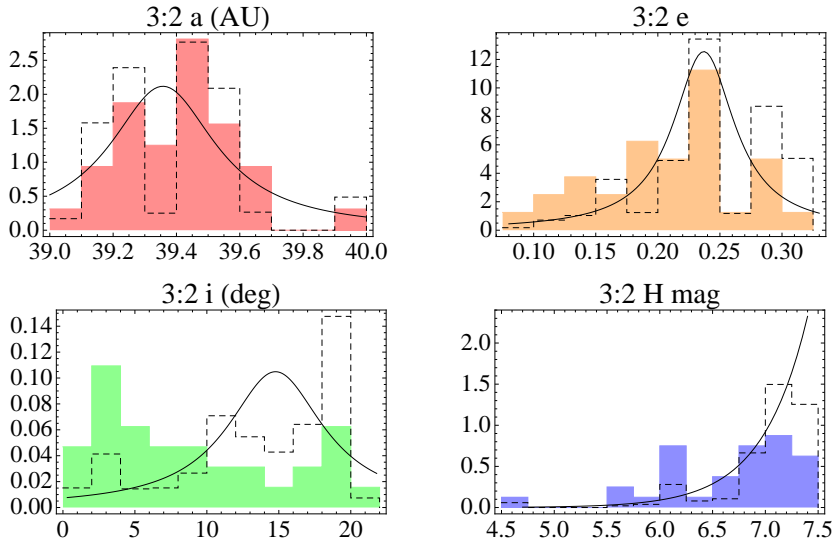


Fig. 4.— Maximum likelihood fit to 32 3:2 objects with  $m_d \leq 23$ , and  $4 \leq H \leq 7.5$ . The filled histogram shows the observed distribution, while the dashed histogram shows the amount by which the distribution is adjusted to account for discovery probabilities. The black lines show the best maximum likelihood fit to each parameter.

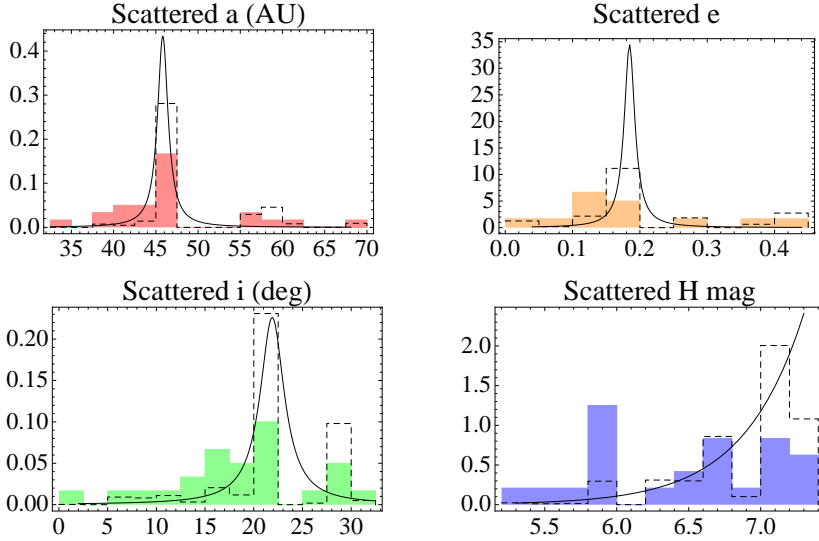


Fig. 5.— Maximum likelihood fit to 24 Scattered objects with  $m_d \leq 23$ , and  $H \leq 7.5$ . The filled histogram shows the observed distribution, while the dashed histogram shows the amount by which the distribution is adjusted to account for discovery probabilities. The black lines show the best maximum likelihood fit to each parameter.

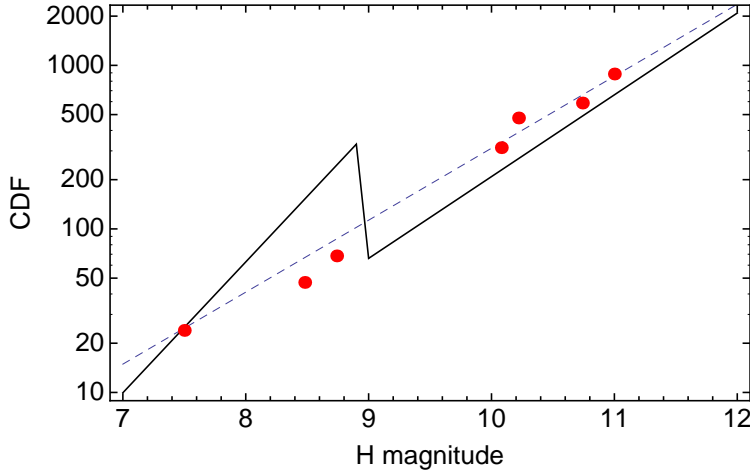


Fig. 6.—  $H$ -magnitude distribution of Centaurs, which are well fit by a single power law with  $\alpha_2 = 0.44 \pm 0.4$  (dashed line). No evidence is found for the divot reported by Shankman et al. (2013), based on 11 CFEPS objects, which is plotted as the black line. (Note that the divot model has been scaled down by a factor of 20 from the absolute scale reported in Petit et al. (2011), to match the values plotted in Shankman et al. (2013).)

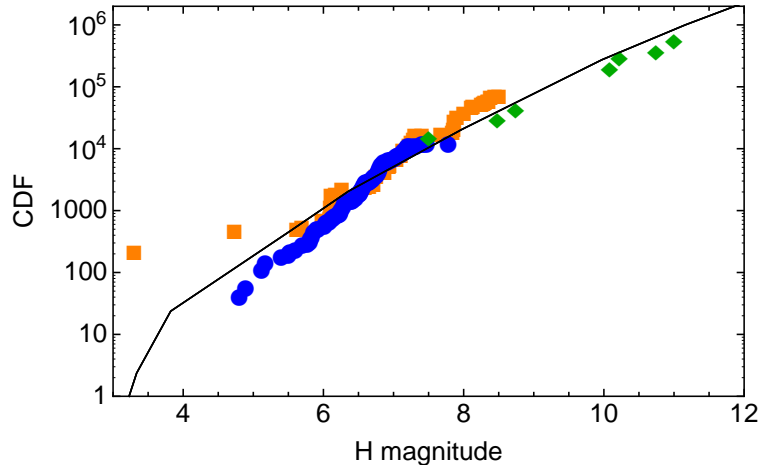


Fig. 7.— Comparison of model of Schlichting et al. (2013) with three classes: Classical (blue circles), 3:2 (orange squares), and Centaur (green diamonds). To match the model predictions, the observations had to be scaled upward by factors of 3 (Classical), 12 (3:2), and 600 (Centaur). Note that the relative ratios between classes is the same as the scales in Table 4, with an overall factor of 3 times greater abundance in the model than we derive from the DES data.